4 Results and discussion

4.1 Site selective fragmentation of D-ribose anions

Monosaccharides represent the most abundant group of biomolecules. They are the subunits of polysaccharides like the energy storage molecules starch and glycogen, and the structural polymer cellulose. Oligosaccharides are involved in important biological functionality, for instance in glycoproteins. The monosaccharides 2-deoxy-D-ribose and D-ribose are bound within the DNA and RNA backbone, respectively. D-ribose is also contained in ATP and NADH, which are critical for the metabolism.

The sugar unit plays a pivotal role in DNA damage since it connects two phosphate groups and a nucleobase, hence a cleavage of any C-O or C-N bond results in a strand break and a base release, respectively. The DNA sugar 2-deoxy-D-ribose was investigated previously with respect to DEA and showed a remarkable sensitivity towards low energy electrons [68]. In the current work the RNA sugar D-ribose has been extensively studied and strong similarities to 2-deoxy-D-ribose have been found. In order to find out if the observed properties can be generalised to other sugars the ketohexose D-fructose has been investigated as well.

4.1.1 Isomers and conformers of D-ribose and D-fructose

2-deoxy-D-ribose and D-ribose are aldopentoses and adopt either a furanose (five-membered) or a pyranose (six-membered) ring structure (figure 4.1). The

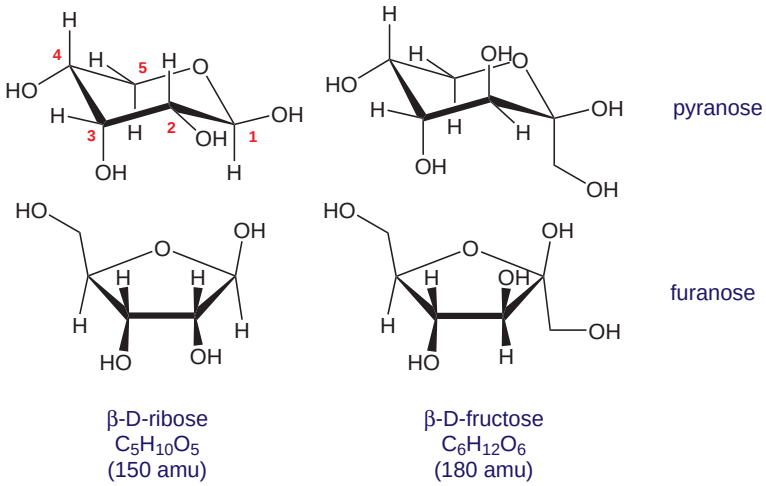

Figure 4.1: Molecular structures of D-ribose and D-fructose in its pyranose and furanose isomers.

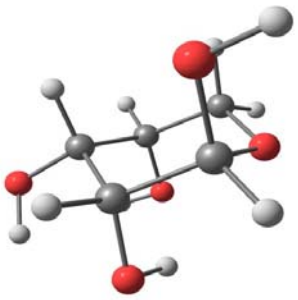

Figure 4.2: Molecular structure of ribopyranose calculated at the B3LYP/6-31++G** level.

pyranose form is the only structure that occurs in crystals [69]. In solution the pyranose predominates but a transformation into the furanose is possible with the linear chain structure as an intermediate. In this case the exact contribution of each possible structure depends on the solvent and its ability to form hydrogen bonds with the different sugar isomers. However, the transformation reaction is solvent-mediated and does not proceed in the gas phase. In the gas phase the thermodynamically most stable structure of D-ribose and 2-deoxy-D-ribose is also the six-membered ring. The stability of the pyranose structure is due to the larger number of hydrogen bonds and the lower steric interaction between adjacent OH groups compared to the furanosic structure [70]. In a pyranose sugar usually three hydrogen bonds contribute to the stabilisation whereas in a furanose in most cases only two H-bonds can be formed. Furthermore, a repulsion between adjacent hydroxyl groups due to dipole and steric interactions is stronger in furanoses, since the dihedral angle (OCCO) is smaller than in pyranoses. It was

shown that the pyranose structure of the crystals is preserved during sublimation at elevated temperatures [70]. Therefore the six-membered ring is assumed to be the only occurring structure in the gas phase.
A computational study of hexoses [71] revealed that the most stable isomer of D-fructose is also the pyranose form. The pyranosic forms of D-ribose and D-fructose differ only in the presence of a methylhydroxy group at the anomeric centre (C1) in D-fructose and the orientation of the second hydroxyl group.

4.1.2 DEA to D-ribose

Fragmentation reactions

Dissociative electron attachment to D-ribose results in manifold fragmentation close to 0 eV (figures 4.3 - 4.11). Main fragmentation products have been observed at 132 amu, 114 amu, 101 amu, 72 amu, 71 amu, 59 amu and 17 amu and are assigned to the following dissociation reactions:

$$\begin{aligned}
e^-(\approx 0\,\mathrm{eV}) + C_5H_{10}O_5 &\rightarrow C_5H_8O_4^- \,(132\,\mathrm{amu}) + H_2O && (4.1)\\
&\rightarrow C_5H_6O_3^- \,(114\,\mathrm{amu}) + 2\,H_2O && (4.2)\\
&\rightarrow C_4H_5O_3^- \,(101\,\mathrm{amu}) + CH_2O + H_2O + H && (4.3)\\
&\rightarrow C_3H_4O_2^- \,(72\,\mathrm{amu}) + H_2O + 2\,CH_2O && (4.4)\\
&\rightarrow C_3H_3O_2^- \,(71\,\mathrm{amu}) + H_2O + 2\,CH_2O + H && (4.5)\\
&\rightarrow C_2H_3O_2^- \,(59\,\mathrm{amu}) + 3\,CH_2O + H && (4.6)\\
&\rightarrow OH^- \,(17\,\mathrm{amu}) + C_5H_9O_4 && (4.7)
\end{aligned}$$

The assignment of fragment ions is in some cases ambiguous (see below), but the use of the three different isotope labelled molecules 5-^{13}C-D-ribose, 1-^{13}C-D-ribose and *C*-1-D-D-ribose (figure 4.5) helped to identify the anionic fragments unambiguously.

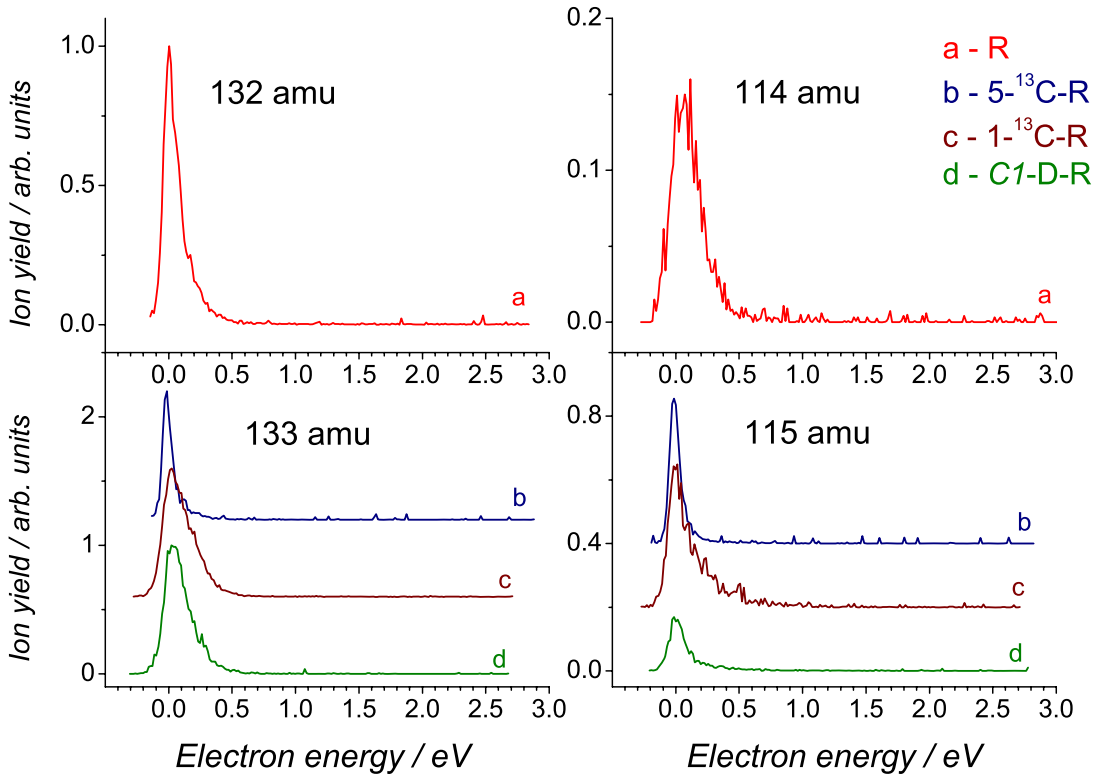

Figure 4.3: DEA spectra of D-ribose at 132 and 114 amu that are due to loss of one or two water molecules, respectively. In the lower panel the corresponding spectra of isotope labelled D-ribose are shown.

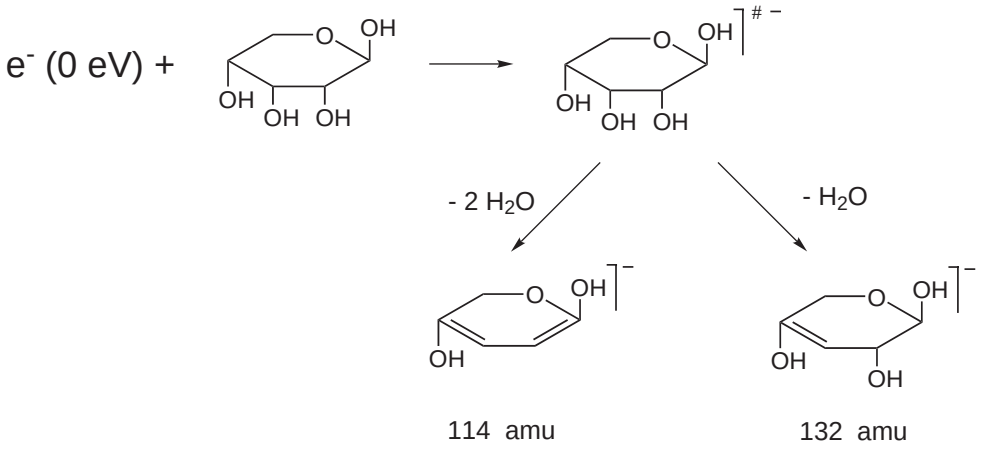

Figure 4.4: Loss of one and two water molecules, respectively, from the D-ribose transient negative ion.

The experiment does not deliver information on the neutral decomposition products, but a comparison of fragment masses in negative ion mass spectra of D-ribose and D-fructose (section 4.1.5) reveals a regular fragmentation pattern associated with loss of different numbers of 18 or 30 amu units, respectively. This is particularly true for the MALDI spectra reported in section 4.1.3. Therefore, the fragmentation reactions in equation 4.1 - 4.7 are tentatively assigned to the production of neutral H_2O and CH_2O molecules.

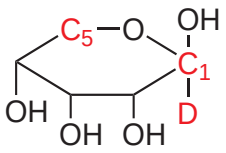

Figure 4.5: Simplified molecular structure of D-ribose. Positions 1 and 5 are indicated which have been labeled with ^{13}C or D, respectively.

As expected for water abstraction, the signals at 132 and 114 amu (red curves in figure 4.3) are completely shifted to 133 and 115 amu in the isotopomers containing ^{13}C (blue and brown graphs). The same shift is observed in *C*-1-D-D-ribose (green) indicating that the deuterium is not involved in H_2O formation. Abstraction of a water unit results in double bond formation in the sugar ring as it is depicted in figure 4.4. Considering typical bond dissociation energies of C-OH and CO-H bonds (4.0 eV and 4.5 eV, respectively [57]) and assuming that a C=C double bond is formed ($\approx$ 3 eV) in addition to the H_2O molecule (D_0(HO-H) = 5.2 eV [57]), one arrives at a thermodynamic threshold of $\Delta H_0 = 0.3\,\text{eV} - EA(C_5H_8O_4)$. The reaction proceeds close to 0 eV, thus the electron binding energy of $C_5H_8O_4$ must be at least 0.3 eV.

The fragment with mass 101 amu can in general be assigned either to $C_5H_9O_2^-$ or $C_4H_5O_3^-$. The first formula contains all five carbon atoms of the sugar ring whereas the second formula is due to an abstraction of a carbon containing fragment. The spectra in figure 4.6 show that the signals at 101 and 102 amu are identical for non-labeled D-ribose (red) and 5-^{13}C-D-ribose (blue), i.e., no shift at all is observed upon labelling with ^{13}C at C5. On the other hand the peak at 101 amu is completely shifted to 102 in 1-^{13}C-D-ribose (brown) and *C*-1-D-D-ribose (green). Consequently C5 must be excised in the course of fragmentation

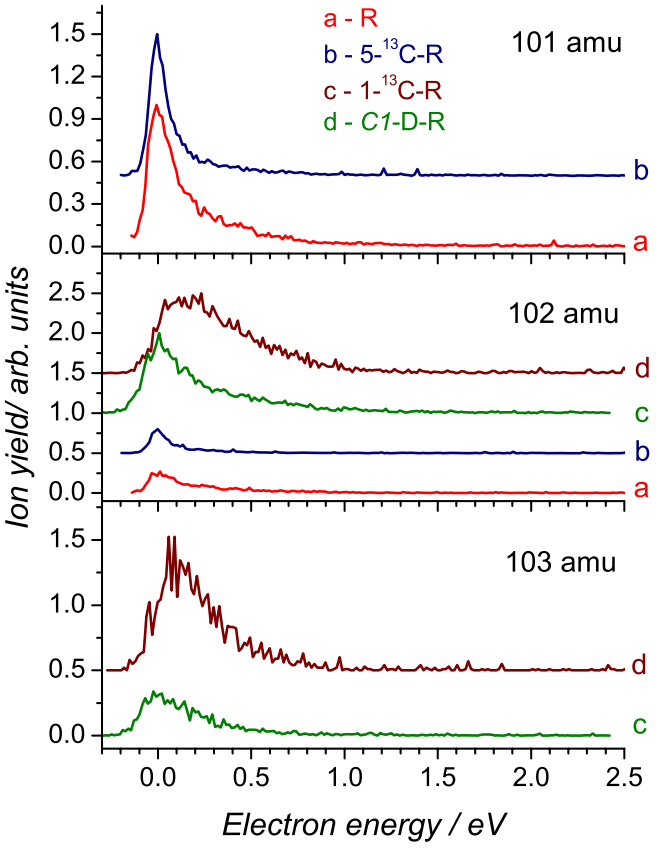

Figure 4.6: Ion yield of 101, 102 and 103 amu following electron attachment to D-ribose and its isotope labelled analogues.

of the D-ribose temporary negative ion. Thus the first sum formula can be excluded and, more specifically, the fragment ion $C_4H_5O_3^-$ does not contain the carbon atom from position 5 (figure 4.7).

The composition of the neutral fragments is not directly accessible from the present experiment. For the generation of $C_4H_5O_3^-$ - that is the excission of C5 from the sugar ring - also the neutral channel $CO_2 + 2\,H_2 + H$ is thermodynamically possible (sum of heats of formation of neutral products $\sum_{neutr.prod.} \Delta H_f^0 =$ -176 kJ/mol [72], see appendix A for a table of heats of formation of relevant compounds), but unlikely due to a large activation barrier. The neutral decomposition channel assigned in equation 4.3 is less favourable in energy ($\sum_{neutr.prod.} \Delta H_f^0 =$ -140 kJ/mol, but a water and a formaldehyde molecule can be formed from the

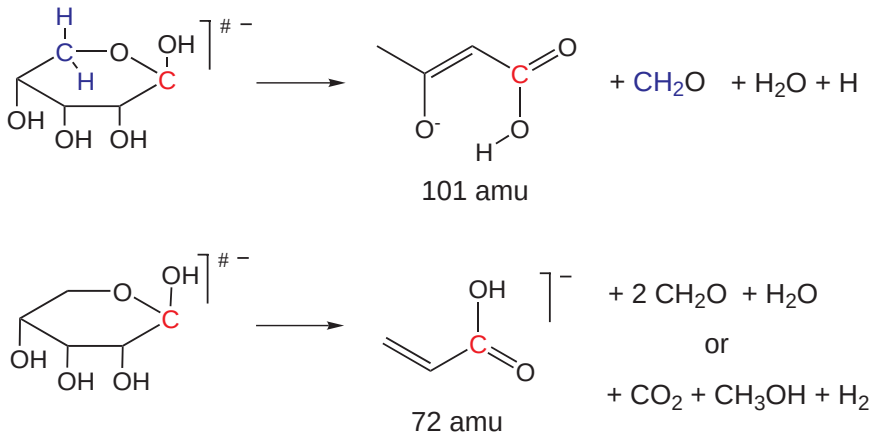

Figure 4.7: Generation of the 101 amu and 72 amu fragment anions by abstraction of neutral water and formaldehyde molecules from the D-ribose transient negative ion.

ring structure of the sugar molecule with presumably lower barriers. In this case formaldehyde is generated from C5 and the negative charge remains on the C1 site (figure 4.7); the hydrogen atom can be abstracted from one hydroxy group where the negative charge is located.

The molecular structure of the $C_4H_5O_3^-$ ion may be a linear chain, but also a five membered ring containing one oxygen atom. Calculations on nine possible structures of $C_4H_5O_3^-$ (see appendix B, figure B.2) performed at the B3LYP/6-31++G** level revealed that only one structure is stable enough to be formed at zero eV (figure 4.13). The anion contains a carboxyl group and is stabilised by an intramolecular hydrogen bond. The electron affinity of the corresponding neutral molecule is remarkably high with 3.9 eV. All other possible geometries for $C_4H_5O_3^-$ are at least 1.9 eV higher in energy than the one shown in figure 4.13. According to the DFT calculations both neutral channels discussed above are thermodynamically possible at zero eV for this particular anion, but the formation of formaldehyde and water most likely requires lower activation barriers.

A similar site selectivity as for the 101 amu fragment is observed for the 71 and 72 amu signals (figure 4.8). The spectra of 5-^{13}C-D-ribose (left panel of figure 4.8) are identical to the respective ones of non-labelled D-ribose (not shown here).

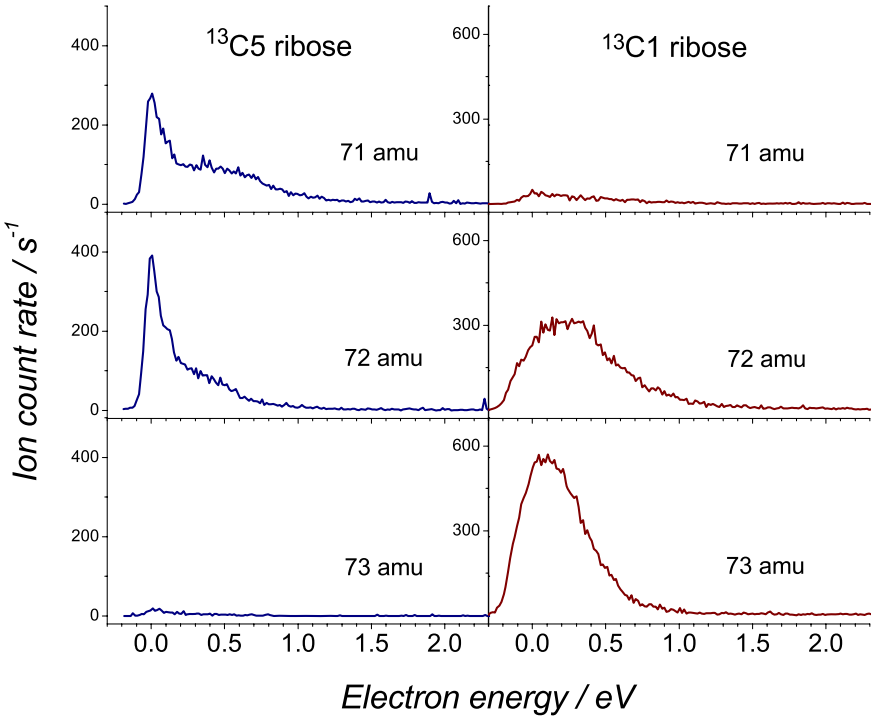

Figure 4.8: Ion yield of 71, 72 and 73 amu following electron attachment to 5-^{13}C-D-ribose and 1-^{13}C-D-ribose.

However, almost no intensity is observed at 71 amu in 1-^{13}C-D-ribose (right panel of figure 4.8) in contrast to a very weak signal at 73 amu in 5-^{13}C-D-ribose, that is attributed to the natural abundance of ^{13}C (3 %).

The 72 amu fragment anion may be generated by loss of two formaldehyde molecules and one water molecule. The observed selectivity suggests that the formaldehyde molecules are formed from C5 and C4, respectively (figure 4.7). However, from thermodynamics the production of CO_2, CH_3OH and H_2 is more favourable ($\sum_{neutr.prod.} \Delta H_f^0 = -595\,\mathrm{kJ/mol}$ compared to $\sum_{neutr.prod.} \Delta H_f^0 = -474\,\mathrm{kJ/mol}$ for production of formaldehyde and water). DFT calculations predict three stable anions (appendix B, figure B.1), that are very close in energy; the most stable one is the anion of propenoic acid and is shown in figure 4.10. According to the DFT calculations only the neutral channel CO_2, CH_3OH and H_2 is exothermic at zero eV electron energy, the formation of two formaldehyde and one water molecule

is endothermic by 478 meV (figure 4.10). On the other hand the spectra shown in figure 4.8 show very broad signals with ion formation up to 1 eV, hence both reactions may contribute.

The formation of the 72 amu fragment proceeds with cross sections close to $10^{-20}\,m^2$; hence it is the dominant fragment anion in DEA to D-ribose (table 4.1).

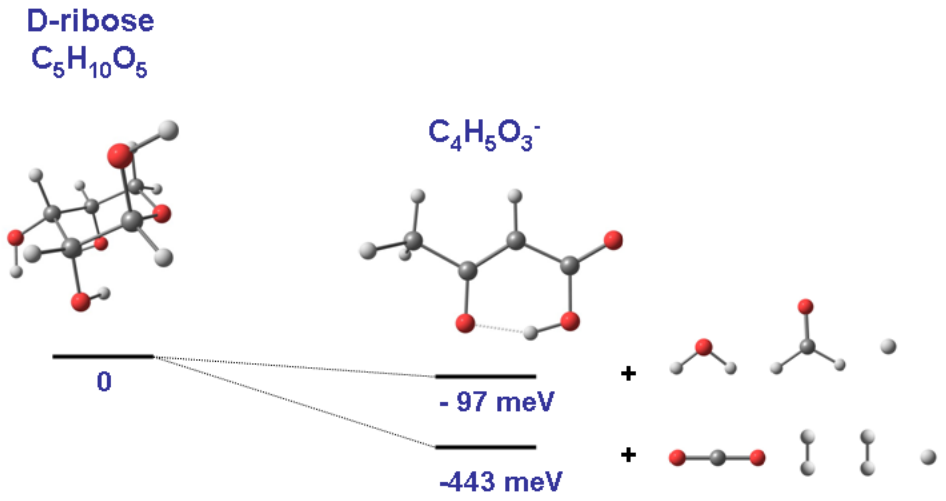

Figure 4.9: Thermodynamic threshold of $C_4H_5O_3^-$ (101 amu) formation with two alternative neutral decomposition channels calculated at the B3LYP/6-31++G** level at 0 K with ZPE.

At 58 and 59 amu the ions $C_2H_2O_2^-$ and $C_2H_3O_2^-$, respectively, are observed (figure 4.11), which can be produced by abstraction of three formaldehyde units from the D-ribose TNI. In addition to the signal close to zero eV the 59 amu fragment is also generated through a higher energy resonance located at 6 - 8 eV. The site selectivity of these reactions is less pronounced than for the higher mass fragments. Nevertheless, the tendency remains the same: In 5-^{13}C-D-ribose the lower energy peak is only slightly shifted to 60 amu, in 1-^{13}C-D-ribose most of the 0 eV signal appears at 60 amu. Finally, for *C*-1-D-D-ribose both spectra at 59 and 60 amu exhibit the same signal intensities indicating that some hydrogen scrambling takes place. Nevertheless the shift in the molecules labelled at C1 is stronger than one can expect for a purely statistical distribution, i.e. a maximum

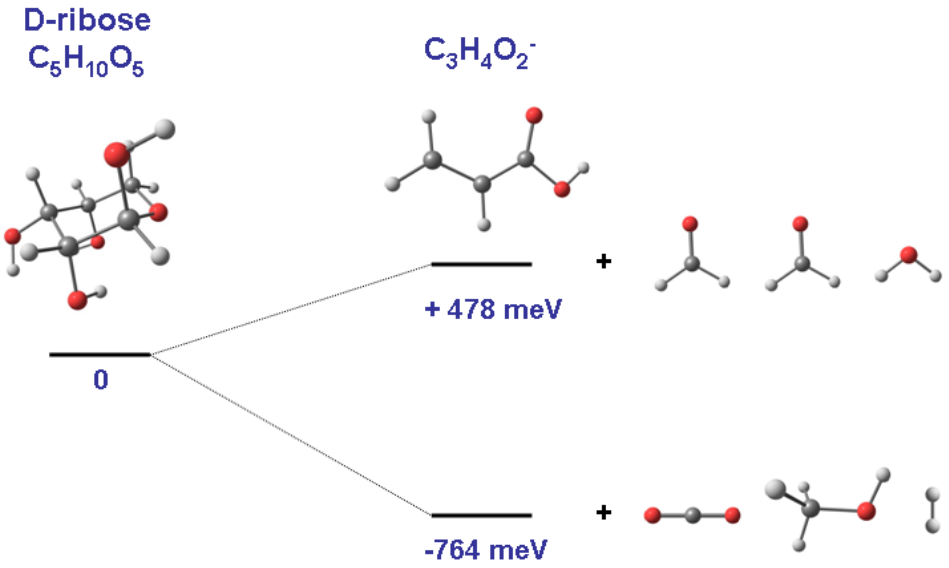

Figure 4.10: Thermodynamic threshold of $C_3H_4O_2^-$ (72 amu) formation with two alternative neutral decomposition channels calculated at the B3LYP/6-31++G** level at 0 K with ZPE.

shift of 40 %. In general the site selectivity is more pronounced close to zero eV than at higher energies.

The structure of $C_2H_3O_2^-$ (59 amu) may be assigned to the stable acetate anion CH_3COO^-. On the other hand, if one follows the line for the other fragmentation reactions and assumes an abstraction of three formaldehyde molecules, it is more likely that the two oxygen atoms are bound to two different carbon atoms forming an enolate $(OH)HC{=}CHO^-$.

A fragment ion that can basically be generated by a single bond cleavage is the OH^- ion (figure 4.12). It was observed at 0.2 eV and with a weaker contribution around 7 eV. The thermodynamic threshold can be estimated to be $\Delta H_0 = D_0$(C-OH) - EA(OH) = 4.0 eV - 1.83 eV = 2.17 eV. Since the reaction occurs already at 0.2 eV, the OH^- ion cannot result from a single bond cleavage leaving the rest of the molecule unchanged, but rather from complex rearrangements generating thermodynamically stable products during OH^- formation.

In table 4.1 the estimated cross sections for the generation of the main fragment

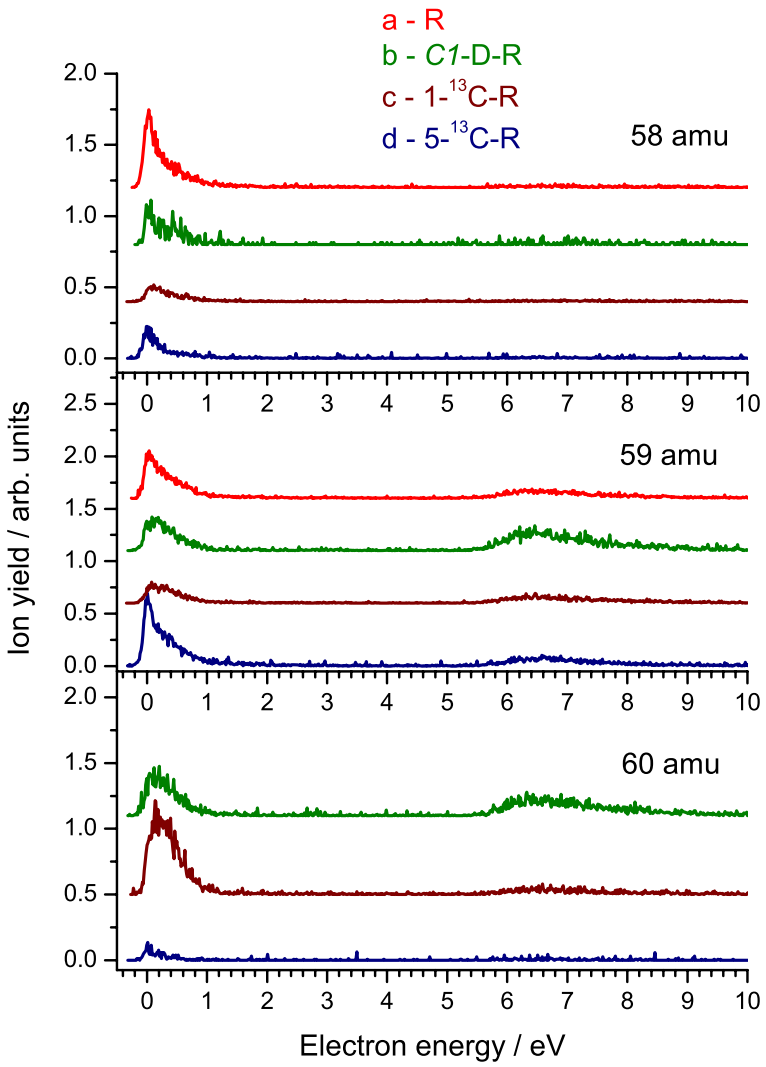

Figure 4.11: Ion yield curves of 58, 59 and 60 amu following electron attachment to D-ribose and its isotope labelled analogues.

anions are summarised; they are in the order of 10^{-21} m^2.

In addition to the reactions discussed above other fragment anions have been observed with weaker intensities at 120, 107, 89 and 84 amu. The 89 amu fragment ion will be discussed in section 4.1.3.

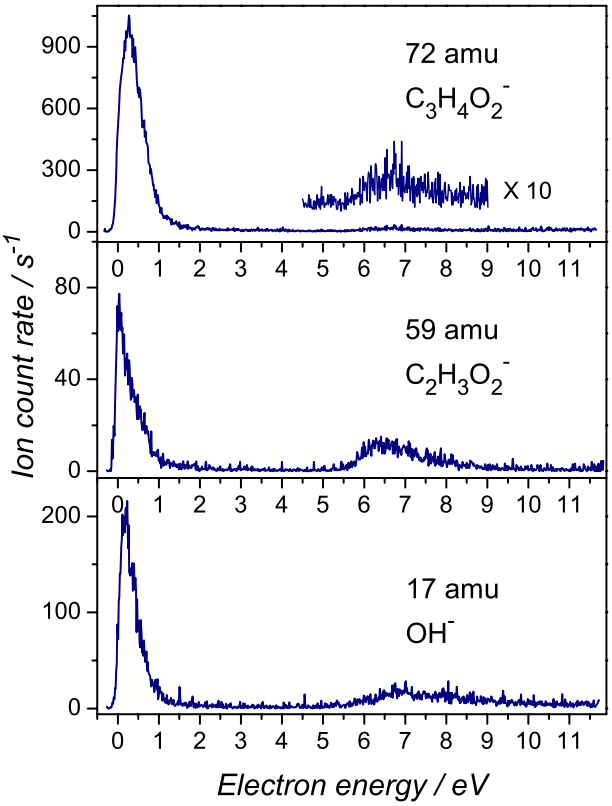

Figure 4.12: Ion yield curves at 72 amu, 59 amu and 17 amu with an expanded energy scale. These fragment anions are also generated at 6 - 8 eV.

Mechanism of ion generation

Near 0 eV signals. D-ribose is a saturated molecule, hence the virtual orbitals are σ^* orbitals, which are expected to be too high in energy to be accessible for electrons having an energy close to zero eV. Recently a weak σ^*_{OH} shape resonance was observed in DEA to methanol and ethanol located at 2.99 and 2.88 eV, respectively [73]. This resonance was observed in the $[M\text{-}H]^-$ ion yield curve and the intensity of the signal is substantially increased in the cyclic alcohol tetrahydrofuran-3-ol and becomes even dominant if two hydroxyl groups are present as in cyclopentane-1,2-diol [73]. Furthermore the onset of the signals is shifted to lower energies (2.50 eV in tetrahydrofuran-3-ol and 1.94 eV in *cis*-cyclopentane-1,2-diol), which is due to a decreasing thermodynamical threshold.

mass / amu	fragment ion	cross section / $10^{-21}\,m^2$
132	$C_5H_8O_4^-$	4
114	$C_5H_6O_3^-$	1
102	$C_4H_6O_3^-$	0.6
101	$C_4H_5O_3^-$	1
72	$C_3H_4O_2^-$	9
71	$C_3H_3O_2^-$	5
59	$C_2H_3O_2^-$	0.5

Table 4.1: Estimated cross sections of the main fragment anions created through DEA to D-ribose.

The increase in intensity may be explained by a decreasing autodetachment width with decreasing energy of the σ^* resonance. This trend could be continued for 2-deoxy-D-ribose and D-ribose, which contain three and four hydroxyl groups, respectively. However, it is not likely that the vertical attachment energy is as low as 0 eV in the sugar molecule.

From the present experiments it can be concluded, that (a) a transient negative ion of D-ribose must be generated, that possesses an electron affinity above or at least equal to 0 eV and that is probably *not* a shape resonance, (b) all fragment anions can be generated at zero eV and must thus posses a high electron affinity, (c) the antibonding states that finally lead to dissociation must be reached by the extra electron with very low barriers from the transient intermediate.

A possible explanation is the initial formation of a vibrational Feshbach resonance, which can be supported by the large dipole moment of the sugar molecule. The electron is attracted by the positive site of the dipole and gets trapped in a very diffuse Rydberg-like orbital by effective transfer of electronic into vibrational energy thereby forming a dipole-bound state (DBS) [74]. Such a vibrationally excited DB-state can couple to a valence state, which then leads to dissociation.

This is a non-Born-Oppenheimer process, as the intramolecular charge transfer strongly influences the geometry of the ion. It was shown theoretically by Sommerfeld [75], that this mechanism is basically possible for D-fructose (see section 4.1.5 and figure 4.21) assuming that the barrier for the intramolecular charge transfer is low enough.

Signals at 6-8 eV. In addition to the signals near 0 eV, the 72 amu and 59 amu fragment ions and OH^- are also generated at higher energies around 7 eV (figure 4.12).

In this energy region electronic excitation is possible and the resonance may be associated with a core excited resonance. A detailed study of DEA and photoelectron spectra of different alcohols containing one or two hydroxyl groups revealed Feshbach resonances located at 6 - 12 eV [73] with two electrons residing in diffuse Rydberg-like orbitals. In the investigated cyclic alcohols mainly two features occurred at 6 - 9 eV that are assigned to an excitation of an electron of either the lone pair of a hydroxyl oxygen (n_{OH}) or a σ_{C-H} orbital [73]. The generation of such Feshbach resonances may also take place in D-ribose.

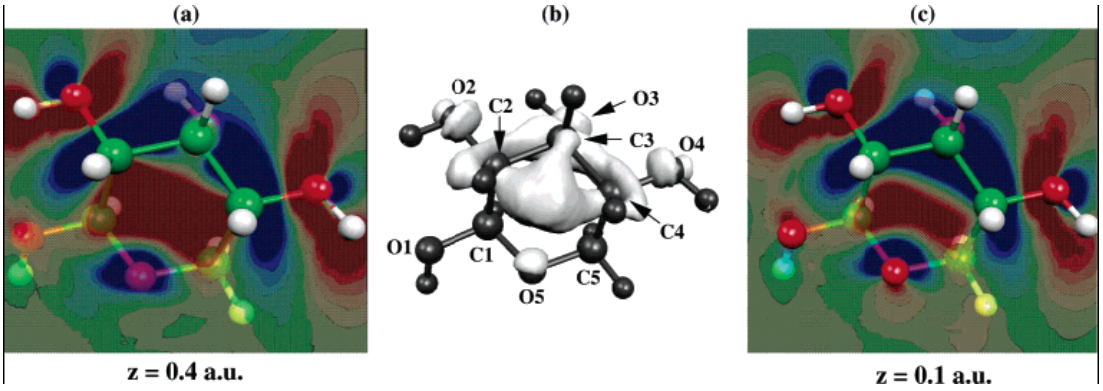

Figure 4.13: Contour plots (a and c) and density map (c) for the resonance state at 7.98 eV in D-ribose (taken from [76]). The electron is localised on the C2-C3-C4 region and on four oxygen atoms; the corresponding C-C and C-OH bonds exhibit a clear antibonding character.

On the other hand calculations on electron scattering on D-ribose [76] revealed

shape resonances at higher energies. For the β-D-ribopyranose four negative ion resonances have been identified between 7.98 eV and 9.49 eV having long enough lifetimes to lead to dissociation. Moreover an analysis of the spatial distribution of the extra electron in these four states shows antibonding nodal planes across the C-OH and C-C bonds (figure 4.13) leading possibly to OH^- formation and breaking of the ring associated with the production of fragment anions containing two or three carbon atoms. This is consistent with the experimental findings; however, no electronic excitation was included in the calculations reported in [76]. Therefore it is most likely that both shape resonances and core excited Feshbach resonances as described in the preceding paragraph contribute to anion formation at energies of 6 - 8 eV.

Possibility of thermal decomposition

It should be noted that a possible thermal decomposition of the sugar molecules was considered, since the generation of fragment radicals could lead to associative attachment, resulting in zero eV signals. This can be excluded due to different reasons: (a) The actual measurements have been carried out at 370 K. To check for thermal decomposition the sample was heated up to 410 K and the ion intensity of heavy and light fragment anions was recorded. No noticeable change in the intensity ratios was observed as it would be anticipated for thermal decomposition at elevated temperatures. (b) A thermal decomposition study of D-fructose [77] reported that the first chemical change occurs at around 100 °C and is a condensation reaction generating oligosaccharides and water; a decomposition of the carbon ring was observed only above 120 °C. Water formation was indeed observed at temperatures above 100 °C in positive ion mass spectra and characteristic O^- ion production around 7 eV. All other ions have been observed already at $\approx$ 80 °C. (c) Negative ion mass spectra of D-ribose and D-fructose (see chapter 4.1.3) using MALDI show similar characteristic signals, which are con-

sistent with DEA spectra. (d) DEA spectra of tetraacetyl-D-ribose (TAR, see chapter 4.2) show threshold signals as well having probably the same origin like the signals in D-ribose. The TAR molecule was evaporated at temperatures as low as 330 K and a careful mass spectrometric analysis ensured that only intact molecules have been present in the gas phase (chapter 4.2).

4.1.3 Negative ion formation in D-ribose probed by MALDI

Metastable decay of [R-H]$^-$

In figure 4.14 (upper panel) the metastable decay spectrum of deprotonated D-ribose is displayed, which proceeds within ≈ 0.5 - 30 μs. Deprotonation occurs most likely at the hydroxy group of the anomeric centre (C1), since this is the most acidic hydroxy group [78]. Deprotonation enables a ring opening as it is shown in figure 4.15. Both the open chain and the closed ring anion may be the precursors for dissociation. The fragmentation pattern of [R-H]$^-$ is very similar to the decomposition of the TNI R$^{-\#}$, i.e. abstraction of different numbers of water and formaldehyde molecules:

$$[\mathrm{R-H}]^- \,(149\,\mathrm{amu}) \rightarrow \mathrm{C_5H_7O_4^-}\,(131\,\mathrm{amu}) + \mathrm{H_2O} \quad (4.8)$$

$$\rightarrow \mathrm{C_4H_7O_4^-}\,(119\,\mathrm{amu}) + \mathrm{CH_2O} \quad (4.9)$$

$$\rightarrow \mathrm{C_4H_4O_3^-}\,(100\,\mathrm{amu}) + \mathrm{CH_2O} + \mathrm{H_2O} + \mathrm{H} \quad (4.10)$$

$$\rightarrow \mathrm{C_3H_5O_2^-}\,(89\,\mathrm{amu}) + 2\,\mathrm{CH_2O} \quad (4.11)$$

$$\rightarrow \mathrm{C_3H_3O_2^-}\,(71\,\mathrm{amu}) + \mathrm{H_2O} + 2\,\mathrm{CH_2O} \quad (4.12)$$

Fragmentation of [R-H]$^-$ was reported previously by means of ESI quadrupole time-of-flight tandem mass spectrometry [79].

Compared to anions generated via DEA the relative intensities in MALDI-PSD are quite different; the dominant signals in PSD of [R-H]$^-$ are 131 and 89 amu, whereas 100 and 71 amu occur only weakly. In general the shift of the signals to one mass below the fragments observed in DEA indicates that the fragmentation

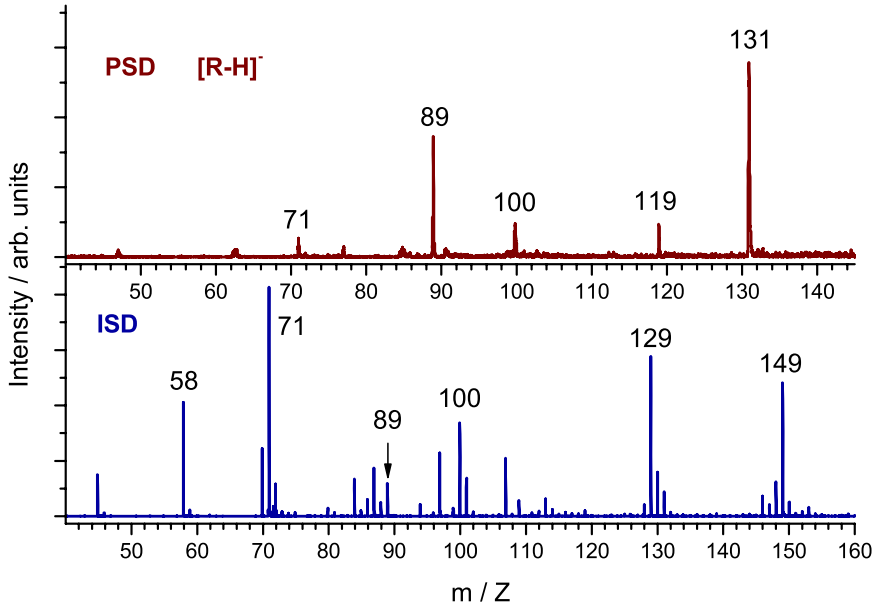

Figure 4.14: Post-source decay (PSD) and in-source decay (ISD) spectra of D-ribose. For PSD the deprotonated D-ribose $[R\text{-}H]^-$ was selected.

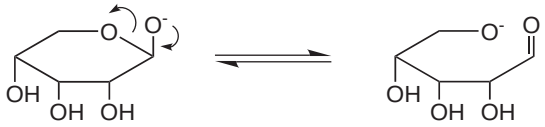

Figure 4.15: Generation of the chain structure by deprotonation.

process of negatively charged D-ribose is mainly governed by the abstraction of *neutral* molecules, rather than the formation of specific anionic products.

The corresponding mass spectra of isotope labelled D-ribose (figure 4.16) show a selective abstraction of a single formaldehyde molecule from C5 yielding 120 and 101 amu in 1-^{13}C-D-ribose and *C*-1-D-D-ribose, respectively. In 5-^{13}C-D-ribose the signals are not shifted and remain at 119 and 100 amu (figure 4.16). This is the same site selectivity that was observed in DEA. On the other hand the fragment ions with lower mass (89 and 71 amu) show a completely different behaviour: In none of the isotope labelled molecules these signals are completely shifted, but a majority of both signals is shifted in 5-^{13}C-D-ribose. In other words, for 89 and 71 amu there are two types of negative ions, one contains C1, but the major part

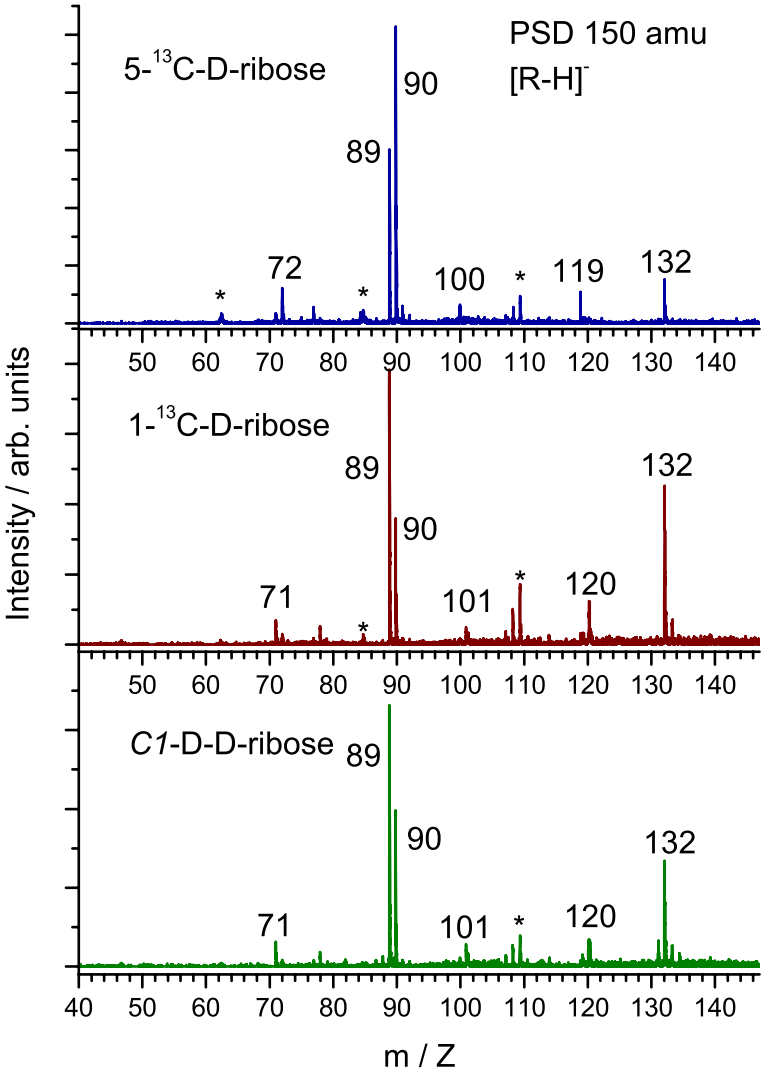

Figure 4.16: MALDI-PSD spectra of $[R\text{-}H]^-$ generated from different isotope labelled analogues.

of negative ions contains C5. This is in contrast to DEA, suggesting that the origin of the 71 amu fragment anion is different in DEA and metastable decay of $[R\text{-}H]^-$.

The PSD spectra indicate that a stepwise decomposition involving metastable $[R\text{-}H]^-$ does not contribute significantly to the fragmentation of the TNI $R^{-\#}$. However, the dominant signal in metastable decay of $[R\text{-}H]^-$ appears at 89 amu, and a weak signal at 89 amu was also observed in DEA (figure 4.17). By compar-

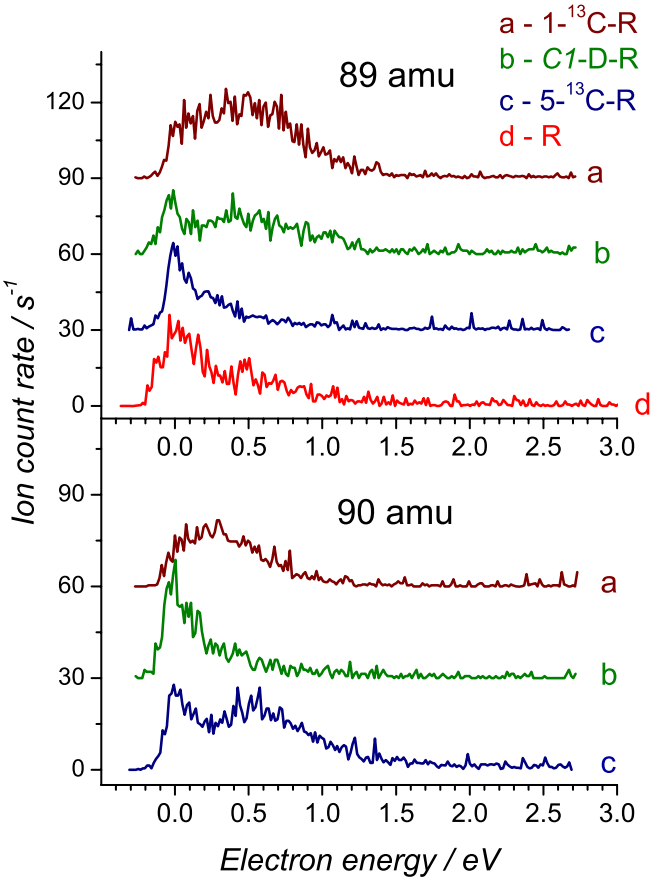

Figure 4.17: Energy dependence of the 89 and 90 amu signals following electron attachment to D-ribose and its isotope labelled analogues.

ing the MALDI and DEA spectra one would expect a signal at 90 amu in DEA of non-labelled D-ribose that is due to abstraction of two formaldehyde molecules from $R^{-\#}$, but this could not be detected. Furthermore the DEA spectra in figure 4.17 do not show a clear selectivity in isotope labelled D-ribose, similar to the 89 amu signal in metastable decay of $[R\text{-}H]^-$ in figure 4.16. It can be concluded that the weak fragment ion at 89 amu produced by DEA to D-ribose is actually a result of a stepwise dissociation with hydrogen abstraction being the initial step followed by metastable loss of two formaldehyde molecules. All other ions in DEA must be generated more directly (see next section).

In-source decay (ISD)

In the in-source-decay (ISD) spectra all ions are detected that are formed within the 400 ns before ion extraction. In the ISD spectrum (figure 4.14, lower panel) the relative intensities of fragment ions are considerably different compared to the PSD spectrum. The dominant fragment ion in ISD of D-ribose is $C_3H_3O_2^-$ at 71 amu, whereas the peaks at 89 and 119 amu disappear almost completely. The 100 amu signal is also stronger than in PSD indicating that these fragments are generated faster than 89 and 119 amu. A completely new signal appears at 58 amu, which is due to:

$$[\mathrm{R}-\mathrm{H}]^- \,(149\,\mathrm{amu}) \rightarrow \mathrm{C_2H_2O_2^-}\,(58\,\mathrm{amu}) + 3\,\mathrm{CH_2O} + \mathrm{H} \qquad (4.13)$$

The ISD spectra of the different isotope labelled D-ribose molecules (figure 4.18) show one general tendency: The negative charge is located at C1 resulting in a shift for the molecules labelled at C1. This is exactly the same tendency we observed in the fragmentation of the TNI $R^{-\#}$, i.e. the abstraction of neutral formaldehyde molecules proceeds from C5.

In general the fragmentation pattern observed in DEA is more similar to the fragmentation in ISD than PSD confirming that direct ion formation can be assumed in DEA of D-ribose without dominant metastable decay processes. The fact that the fragment ions observed in MALDI-ISD are shifted by one mass unit compared to main fragmentation products in DEA reflects the different formation mechanisms of the precursor ion, i.e. the TNI $R^{-\#}$ in DEA and the deprotonated D-ribose $[R\text{-}H]^-$ in MALDI.

However, the mechanism of anion generation in MALDI is not fully understood and it is likely that different processes proceed simultaneously. The ions are formed in the plume, where the density and temperature is high and thus multiple collisions occur. Therefore the conditions are not well-defined and secondary reactions like proton and electron transfer play a crucial role [80]. Electron capture processes are discussed due to the presence of low energy photoelectrons,

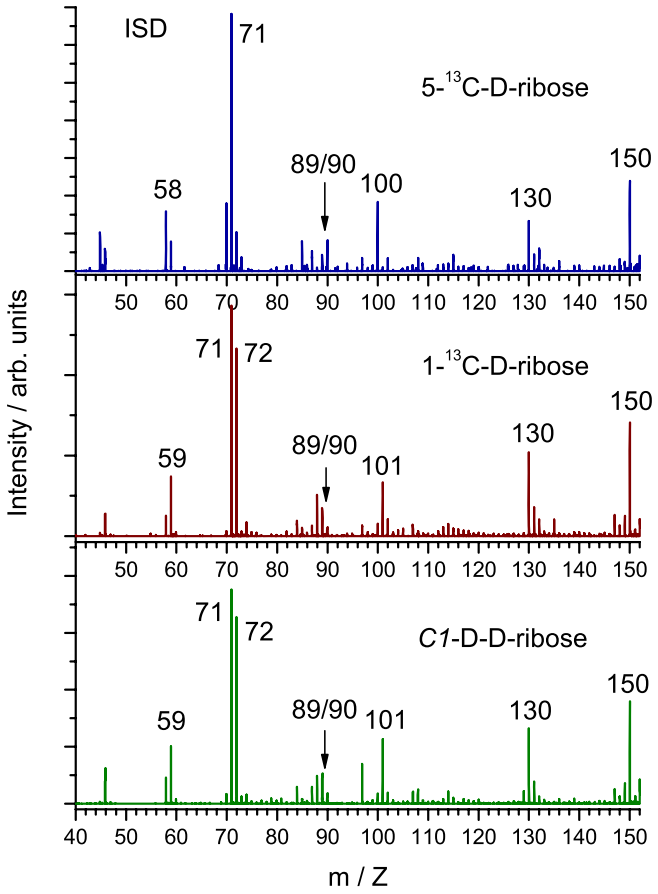

Figure 4.18: MALDI-ISD spectra of different isotope labelled D-ribose molecules.

the existence of which was shown previously by means of SF_6^- production out of SF_6 [81]. Therefore an alternative mechanism of anion formation in MALDI of D-ribose is the capture of 0 eV electrons and subsequent dissociation. Due to the in-plume conditions it is possible that closed shell anions are formed in the course of collisions with surrounding matrix molecules rather than radical anions that dominate in DEA.

4.1.4 Origin of site selectivity

In the DEA experiments as well as in the MALDI spectra of D-ribose a pronounced site selectivity was observed in the sense that neutral formaldehyde is

excised from C5 and negative ion fragments contain C1.

The bond strength of a typical C-C bond is comparable to the bond strength of a C-O bond. However, it was shown that in oxygen-containing heterocycles the endocyclic C-O bond appears to be the weakest site, since the initial step in photo-induced dissociation is a homolytic C-O bond cleavage [82, 83]. Furthermore the structure of the pyranose ring is slightly distorted in order to allow the formation of intramolecular hydrogen bonds what is accompanied with a decrease of the total energy of the sugar. Therefore the most stable structure is a compromise between the formation of stabilising hydrogen bonds and destabilising steric and dipolar repulsion. In D-ribose three intramolecular hydrogen bonds are formed among the hydroxyl groups at C2, C3 and C4, but not C1 [70]. The C5 position is distinct in that it does not have a hydroxyl group and therefore the local bond strength at C1 but particularly at C5 is decreased due to the lack of stabilising hydrogen bonds. The special role of C5 has been shown already in low energy ion reactions with D-ribose [84].

In negative ions generated in DEA and MALDI the fragmentation of the sugar ring is most likely governed by the antibonding character of the initial state of the extra electron. The negative charge becomes most likely localised on one of the hydroxyl groups leading to a more pronounced selectivity for the heavier fragments. Unfortunately, calculations on bound electronic states do not deliver reliable information on virtual states. Therefore more sophisticated calculations have to be performed to elucidate the origin of the site selectivity.

4.1.5 DEA to D-fructose

Experiments on DEA of D-fructose (F) have been performed in Innsbruck using a hemispherical electron monochromator. This molecule was investigated in order to reveal similarities to D-ribose that may allow a generalisation to the reactions of monosaccharides with low energy electrons.

A large number of fragment ions was observed that are generated close to zero eV similar to the signals in D-ribose. In figure 4.19 some selected ion yield curves are displayed, all anions generated at zero eV are shown in a mass spectrum in figure 4.20. The fragmentation pattern is similar to D-ribose, i.e. the parent ion F^- or the parent ion after loss of hydrogen was not observed, but an abstraction of one, two and three water molecules leading to anions at 162, 144 and 126 amu, respectively:

$$e^-(\approx 0\,\mathrm{eV}) + C_6H_{12}O_6 \rightarrow C_6H_{10}O_5^- \,(162\,\mathrm{amu}) + H_2O \quad (4.14)$$

$$\rightarrow C_6H_8O_4^- \,(144\,\mathrm{amu}) + 2\,H_2O \quad (4.15)$$

$$\rightarrow C_6H_6O_3^- \,(126\,\mathrm{amu}) + 3\,H_2O \quad (4.16)$$

The abstraction of a CH_2O molecule - most likely the exocyclic methylhydroxy group - leads to the same fragment anions at 132 and 114 amu already observed with D-ribose:

$$\rightarrow C_5H_8O_4^- \,(132\,\mathrm{amu}) + H_2O + CH_2O \quad (4.17)$$

$$\rightarrow C_5H_6O_3^- \,(114\,\mathrm{amu}) + 2\,H_2O + CH_2O \quad (4.18)$$

On the other hand production of CO_2 and H_2 is thermodynamically more favourable than H_2O and CH_2O, but is assumed to proceed with larger activation barriers than the formation of H_2O and CH_2O.

A further decomposition of the sugar ring similar to the reactions described above is due to the following reactions:

$$\rightarrow C_4H_6O_3^- \,(102\,\mathrm{amu}) + H_2O + 2\,CH_2O \quad (4.19)$$

$$\rightarrow C_4H_5O_3^- \,(101\,\mathrm{amu}) + 2\,CH_2O + H \quad (4.20)$$

$$\rightarrow C_4H_4O_2^- \,(84\,\mathrm{amu}) + 2\,H_2O + 2\,CH_2O \quad (4.21)$$

$$\rightarrow C_3H_4O_2^- \,(72\,\mathrm{amu}) + H_2O + 3\,CH_2O \quad (4.22)$$

$$\rightarrow C_2H_3O_2^- \,(45\,\mathrm{amu}) + \mathrm{fragments} \quad (4.23)$$

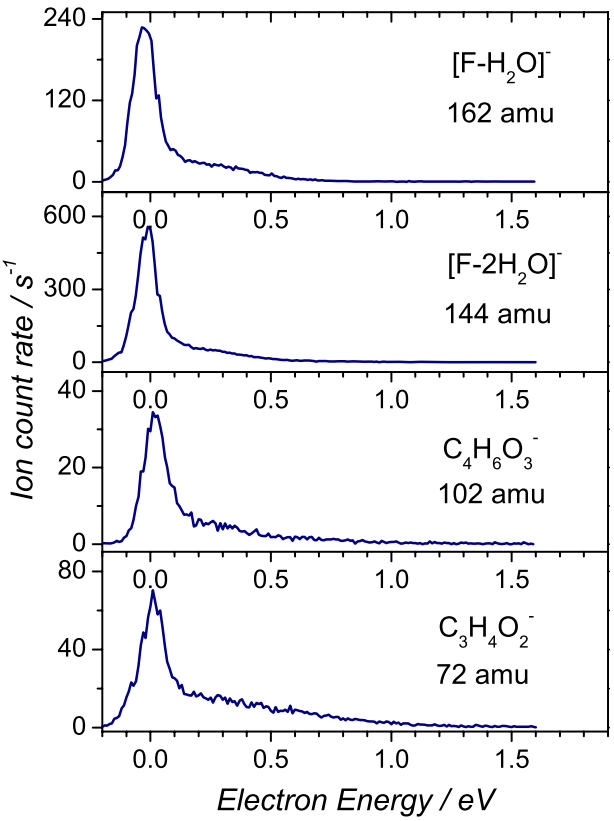

Figure 4.19: Ion yield curves of selected fragment ions generated by electron attachment to D-fructose.

As can be seen in figure 4.20 the formation of the 101 and 102 amu ions are dominant as in D-ribose with stronger contribution of 102 amu. It is likely that the dissociation of the D-fructose TNI leads to the same fragment anions discussed above for D-ribose, however, with slightly different intensity ratios.

All reactions described above occur exclusively close to zero eV. Extended measurements up to 12 eV did not show any signals apart from the ions H^-, OH^- and O^- (see below). Therefore it is assumed that the threshold signals have the same origin discussed in section 4.1.2 for D-ribose. The calculations performed by Sommerfeld [75] revealed that a cyclic D-fructose molecule exists having a dipole moment of 4.05 D, which supports a dipole bound state (DBS) with an electron binding energy of more than 5 meV. The formation of the DBS is de-

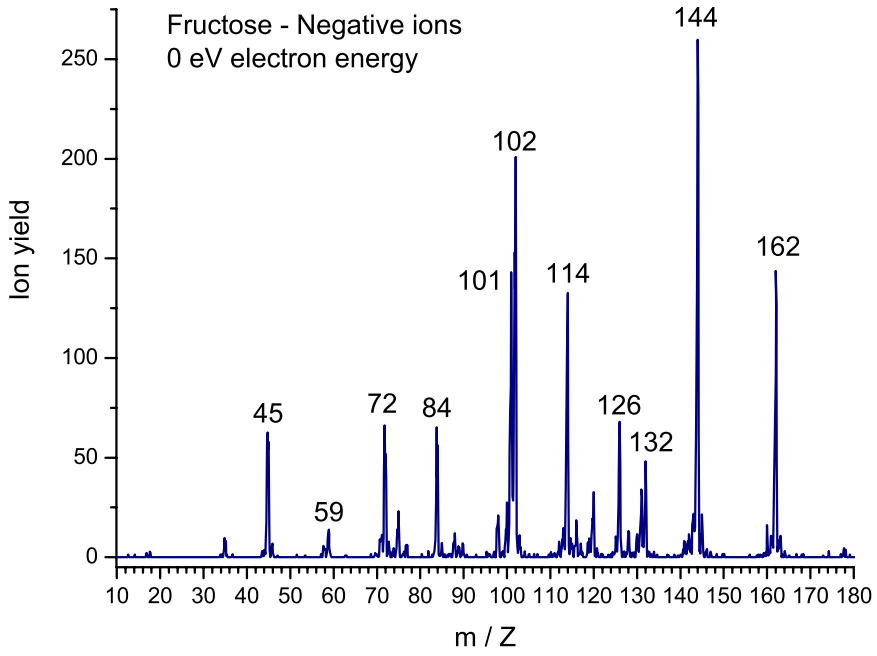

Figure 4.20: DEA mass spectrum of D-fructose recorded at 0 eV electron energy.

picted schematically in figure 4.21. In addition to the DBS a stable *valence* anion was identified possessing a chain structure that is more stable than the neutral D-fructose molecule. Furthermore the abstraction of a water molecule was found to be exothermic if the product ion is an open chain ion. Therefore a fragmentation reaction like the loss of a water molecule from the D-fructose TNI is possible at zero eV, if the coupling between the DBS and the valence anionic state is efficient and the barrier low enough (figure 4.21).

In contrast to the complex reactions described above, H^-, OH^- and O^- may result from simple bond cleavage leaving the rest of the D-fructose molecule unchanged. All these ions have been observed only at higher energies above 5 eV (figure 4.22). From typical bond dissociation energies ($D_{O-H} = 4.5$ eV; $D_{C-OH} = 4.0$ eV) and electron affinities ($EA_H = 0.75$ eV; $EA_{OH} = 1.83$ eV) the thermodynamical threshold for H^- and OH^- generation becomes 3.75 and 2.17 eV, respectively.

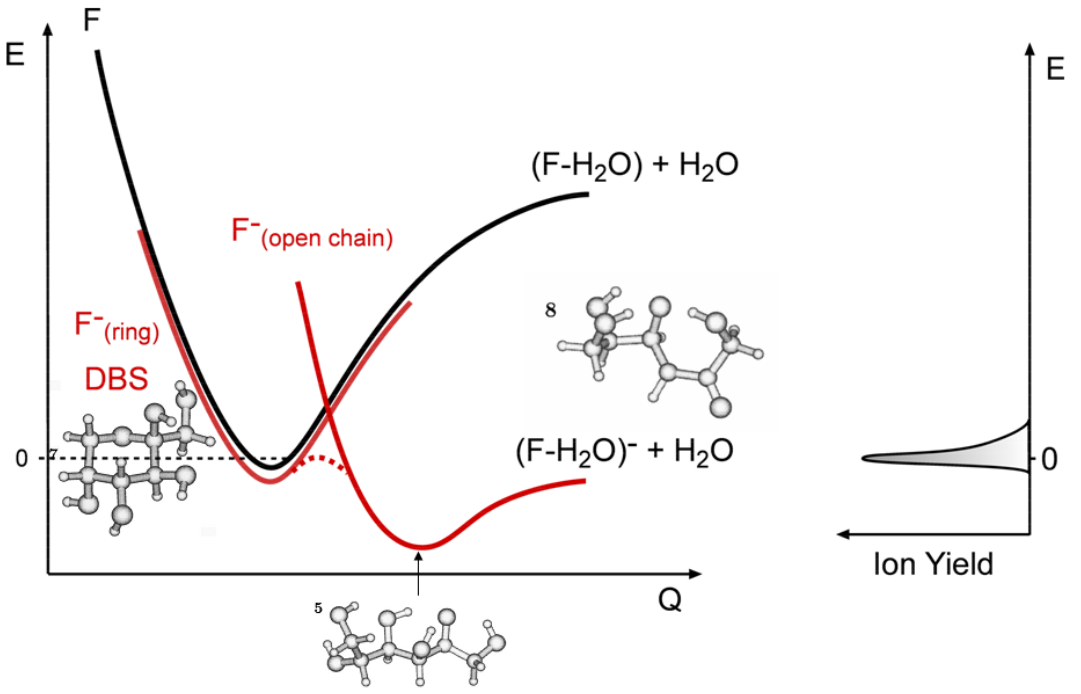

Figure 4.21: Simplified potential energy diagram showing the dipole bound state of D-fructose, that is converted into the open chain valence anion by intramolecular charge transfer, which finally dissociates by abstraction of a water molecule. The anionic structures are taken from Sommerfeld [75].

4.1.6 MALDI of D-fructose

The metastable decay of deprotonated D-fructose $[\text{F-H}]^-$ (figure 4.23) yields the same fragment anions that are observed in post-source decay of D-ribose, i.e. 71 amu, 89 amu, 100 amu, 119 amu and 131 amu (section 4.1.3). The ion yields are almost identical in both spectra, and in PSD of $[\text{F-H}]^-$ additionally 107 amu, 143 amu, 149 amu and 161 amu have been observed:

$$[\text{F}-\text{H}]^- \rightarrow \text{C}_6\text{H}_9\text{O}_5^- \,(161\,\text{amu}) + \text{H}_2\text{O} \tag{4.24}$$

$$\rightarrow \text{C}_5\text{H}_9\text{O}_4^- \,(149\,\text{amu}) + \text{CH}_2\text{O} \tag{4.25}$$

$$\rightarrow \text{C}_6\text{H}_7\text{O}_4^- \,(143\,\text{amu}) + 2\,\text{H}_2\text{O} \tag{4.26}$$

$$\rightarrow \text{C}_3\text{H}_7\text{O}_4^- \,(107\,\text{amu}) + \text{C}_3\text{H}_4\text{O}_2 \tag{4.27}$$

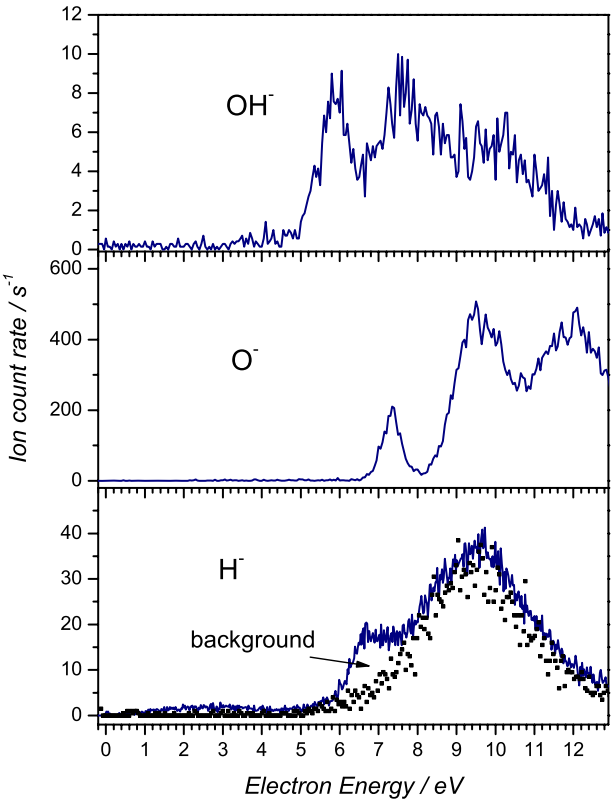

Figure 4.22: Production of OH^-, O^- and H^- through DEA of D-fructose.

The assignment of the reactions 4.24 - 4.26 is unambiguous and the close resemblance of the other signals to the spectrum of D-ribose supports the picture that anions of D-fructose and D-ribose decompose in the same way leading to the same fragment anions.

The lower panel of figure 4.23 shows the ISD spectrum of D-fructose with dominant signals at 179 amu and 101 amu, which are due to $[F\text{-}H]^-$ and $C_4H_5O_3^-$, respectively. It is interesting to note that in PSD $C_4H_4O_3^-$ (100 amu) is generated in contrast to ISD, where $C_4H_5O_3^-$ (101 amu) dominates. Similar to the MALDI spectra of D-ribose the 71 amu signal is stronger in ISD than in PSD indicating a fast fragmentation.

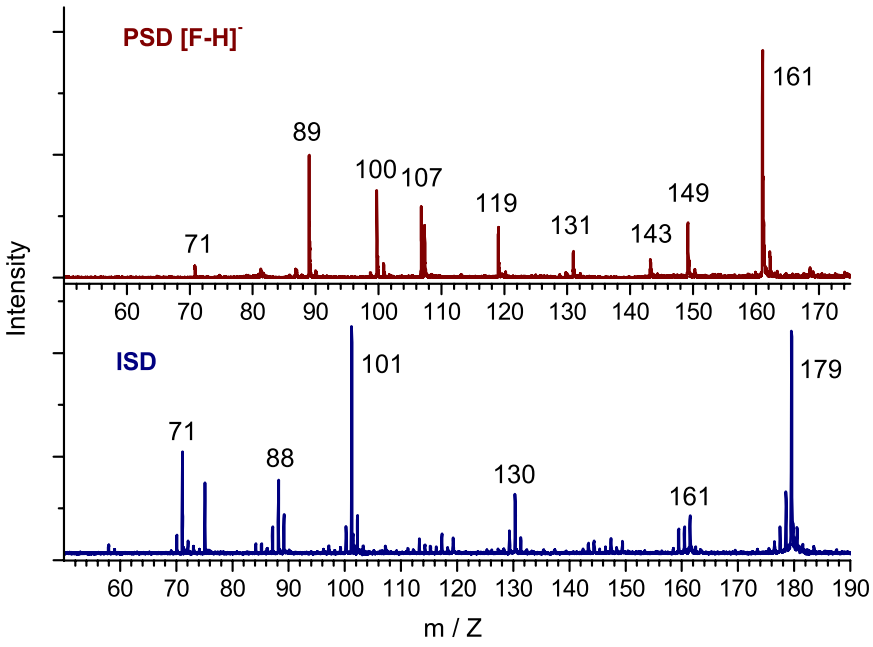

Figure 4.23: Negative ion mass spectra obtained by MALDI. In the upper panel PSD of deprotonated D-fructose ($[F\text{-}H]^-$) is shown and in the lower panel ISD of D-fructose.

4.1.7 Conclusions

The RNA sugar D-ribose efficiently captures electrons close to zero eV followed by a characteristic decomposition, i.e., by loss of different numbers of water and formaldehyde molecules. The use of three different isotope labelled analogues of D-ribose revealed a remarkably site selective excission of C5, most likely as a neutral formaldehyde molecule. This implies a pronounced fragility of the carbon at position 5 in D-ribose towards low energy electrons. C5 in the pyranose sugar is distinct in that it is not bound to a hydroxyl group. This corresponds to C4 in the sugar bound within DNA or RNA, and a release of C4 or C5 corresponds directly to a strand break.

The signals close to zero eV can be explained by the initial formation of a dipole-bound state that serves as a doorway to dissociation at very low energy. Weak signals at 6 - 8 eV are associated with both high lying shape resonances and core excited Feshbach resonances.

The investigation of metastable decay of deprotonated D-ribose by means of MALDI confirms the regular fragmentation pattern of negatively charged monosaccharides, which is governed by the loss of *neutral* fragments. This leads to fragment anions that are usually observed one mass below the corresponding signal in DEA. A comparison of MALDI spectra (in-source decay and post-source decay) with DEA spectra indicates that the fragmentation of the D-ribose temporary negative ion ($R^{-\#}$) proceeds directly and not sequentially with metastable intermediates. The only exception is the weak signal at 89 amu, which is most likely due to an initial formation of metastable $[R\text{-}H]^-$ and subsequent decomposition by loss of two formaldehyde molecules.

DEA experiments on D-fructose yield basically the same results as D-ribose suggesting that a characteristic fragmentation at threshold can be ascribed to all monosaccharides.

4.2 Improving the model of sugar in RNA/DNA: DEA to peracetylated D-ribose

The monosaccharides react readily with low energy electrons resulting in manifold fragmentation with high site selectivity. However, a comparison of the molecular structure of isolated D-ribose with the sugar unit bound within RNA shows clear differences (figure 4.24): (a) In DNA and RNA the sugar units are five-membered rings in contrast to free sugars. It is so far not clear how this influences anion

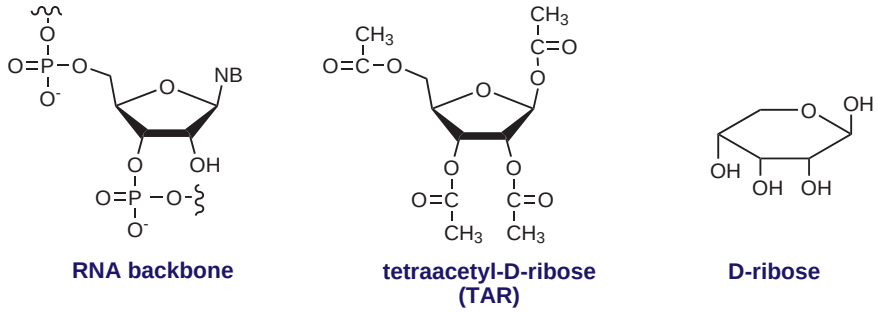

Figure 4.24: Molecular structures of D-ribose bound within RNA, the isolated monosaccharide D-ribose and tetraacetyl-D-ribose.

formation and fragmentation. (b) There are no free hydroxyl groups in DNA and only one in RNA (at C2). The hydroxyl groups at C3 and C5 are bound to phosphate groups, and C1 forms an N-glycosidic bond to a nucleobase. In order to judge the relevance of results obtained with simple subunits it is necessary to investigate systems, which may serve as models to mimic the particular component when coupled in DNA or RNA. To track this question peracetylated D-ribose was studied (tetraacetyl-D-ribose, TAR; figure 4.24). TAR can be obtained in pure furanosic form, i.e. a five-membered ring, and no free hydroxyl groups are present. TAR is therefore considered to be a substantially better model for the sugar unit in DNA.

The presence of acetyl groups increases the vapour pressure of TAR compared

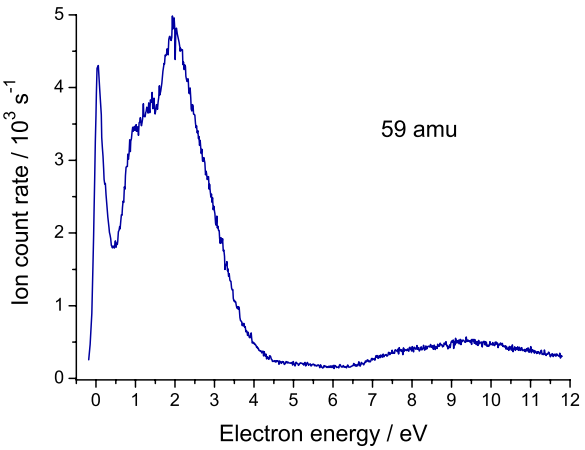

Figure 4.25: Ion yield of CH_3COO^-, the most abundant fragment ion that is generated after electron attachment to TAR.

to D-ribose most likely due to a stronger crystal lattice in D-ribose. Therefore it was possible to obtain anion signals already at temperatures of 330 K, and the operating temperature was 340 - 360 K. In a previous mass spectrometric study [86] a clear discrimination between pyranosic and furanosic isomers of TAR was documented employing a source temperature of 430 K. A positive ion mass spectrum measured in our quadrupole mass spectrometer showed that the sample in fact consisted exclusively of intact furanosic TAR molecules.

4.2.1 Transient negative ions and ion yields

The main fragment anion in DEA of TAR is the acetate anion CH_3COO^- (figure 4.25) at 59 amu that is generated by a simple C-O bond cleavage at C1, C2, C3 or C5. It appears within three energy regions: (1) Within a sharp peak at threshold, (2) between 1 and 3 eV from at least two overlapping resonances, and (3) with lower intensities between 7 and 11 eV.

Another series of fragment ions was observed at 70, 84 and 100 amu (figure 4.26) within a narrow signal close to zero eV and a weak contribution at higher energies.

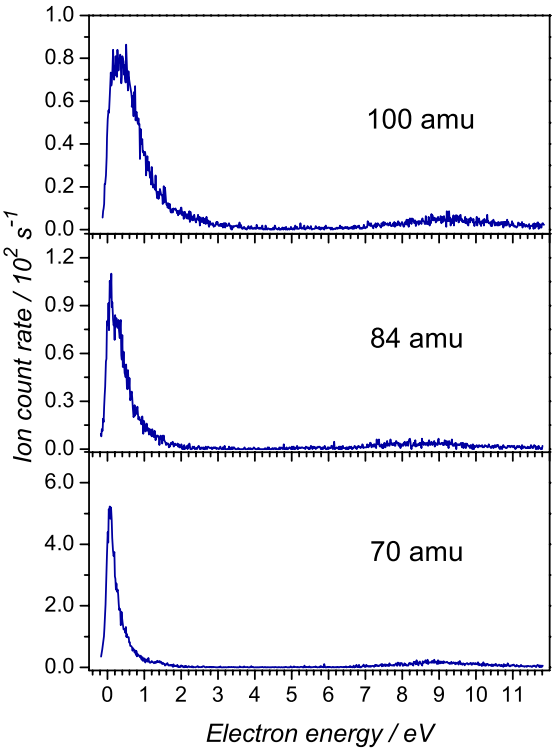

Figure 4.26: Fragment ions at 70, 84 and 100 amu, that are only generated close to zero eV and at 7 - 9 eV. The π^* shape resonance around 2 eV is missing and thus the spectra are very similar to the DEA spectra of isolated D-ribose.

These features are very similar to the spectra of isolated D-ribose, on the other hand these anions are not created through the resonance at 1 - 3 eV that was observed in the ion yield of CH_3COO^-. Due to the lack of low lying π^* orbitals in D-ribose the threshold peak was assigned to a dipole bound state that couples to a σ^* valence state. In TAR, however, empty π^* orbitals from the acetyl groups are present. Therefore the resonances between 1 and 3 eV are tentatively assigned to π^* shape resonances.

A group of heavier fragment ions (116, 119, 154, 215 amu) is generated exclusively through the π^* shape resonance (figure 4.27) located at 1 - 3 eV peaking at 1.6 - 1.8 eV, depending on the respective product ion.

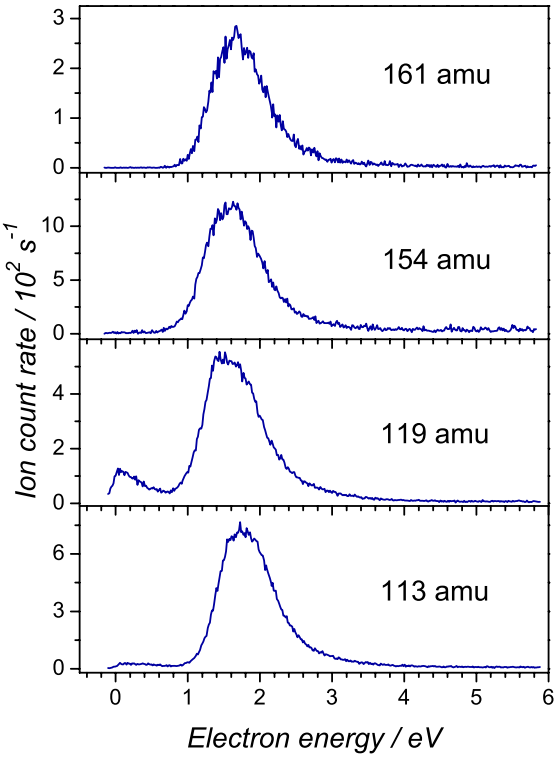

Figure 4.27: Ion yield of heavier fragment anions that are exclusively generated through the π^* shape resonance around 2 eV.

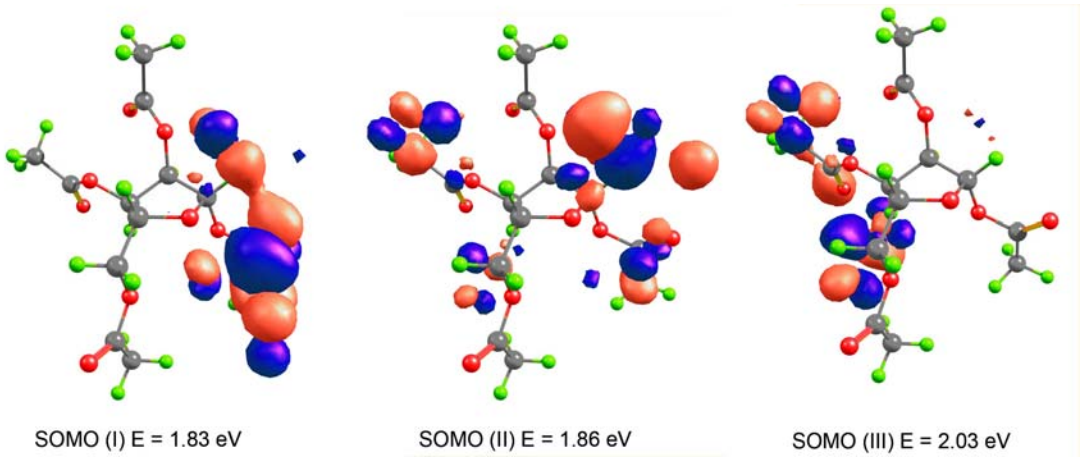

Figure 4.28: Molecular orbital representations of transient negative ions around 2 eV calculated by the stabilisation method. Calculations have been performed by I. Dabkowska [85].

The presence of π^* shape resonances in TAR was confirmed by *ab initio* calculations at HF/6-31+G** level using the stabilisation method [85]. TAR does not possess a positive electron affinity and is thus not able to bind an extra electron in a stable state. However, a shape resonance is a metastable state within the ionisation continuum, in which the electron is quasibound. These states cannot be calculated by means of conventional *ab initio* methods for bound electronic states, since the application of increasingly larger basis sets leads to an increasingly expanded wavefunction finally resulting in the neutral molecule with the extra electron at infinity. Therefore the stabilisation method was used previously to identify metastable states in biomolecules such as nucleotides [20]. In TAR shape resonances have been revealed by means of the stabilisation method [85] at 1.83, 1.86 and 2.03 eV with the negative charge located outside the ring on the acetyl groups (figure 4.28). At lower energies no metastable states could be predicted.

Therefore the threshold peaks must have another origin; the sharp peak close to zero eV in figure 4.25 could be assigned to a hot-band transition to the π^* shape resonance. That is, vibrationally excited molecules capture electrons near 0 eV to form the π^* shape resonance. It has been shown previously [87] that the presence of a shape resonance distinctly off zero eV can lead the appearance of a threshold peak at elevated temperatures. At the temperature of the present experiment only very few molecules are expected to be vibrationally excited. Nevertheless, the Franck-Condon transition from an excited state may lead to a strong signal at low energy due to (a) the reciprocal energy dependence of the electron attachment cross section (see chapter 2.1.3), (b) the smaller energy width of the resonance at lower energy leading to a longer lifetime of the TNI with respect to autodetachment and finally to a higher probability of dissociation according to equation 2.16. However, this mechanism can be excluded for CH_3COO^- production at zero eV, since the threshold peak would show a pronounced temperature dependence. The ion yield for CH_3COO^- was recorded at different tempera-

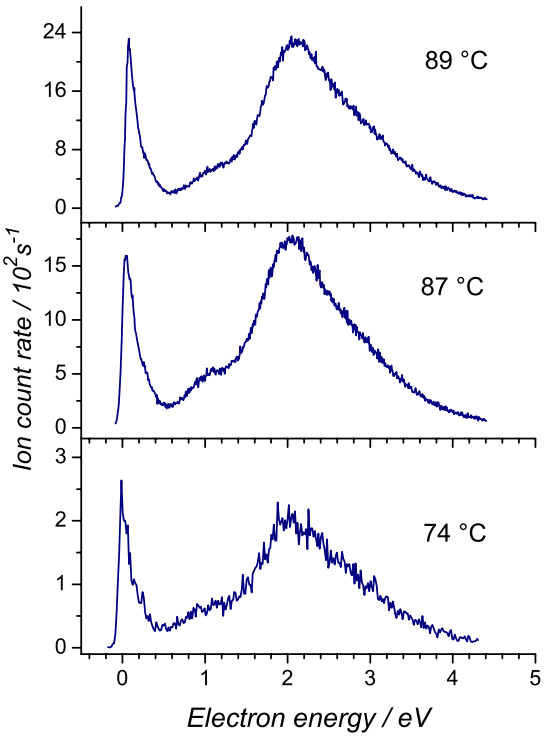

Figure 4.29: Ion yield of CH_3COO^- following electron attachment to TAR at different temperatures. The ion count rate increases according to the increasing vapour pressure, but no change in the relative intensities of the threshold peak and the resonance at 2 eV is noticeable.

tures and no change in relative intensities of the peaks at 0 and 1 - 3 eV could be determined (figure 4.29). For the fragment anions in figure 4.26 no π^* shape resonances were observed and therefore no hot band transitions are expected. Therefore there is no other explanation for the threshold peaks than the initial formation of a dipole bound state followed by dissociation through a valence state similar to D-ribose and D-fructose.

4.2.2 Decomposition pathways

The acetate anion CH_3COO^- can be formed by a single C-O bond cleavage. The electron affinity of the CH_3COO radical is 3.47 eV [72] and thus in the same order like the C-O bond that is broken, making the reaction energetically accessible at 0 eV electron energy.

The assignment of the fragment ions at 70, 84 and 100 amu to a stoichiometric composition is ambiguous since the products may contain either four or five carbon atoms:

$$e^- + \mathrm{TAR} \rightarrow \mathrm{C_4H_4O_3^-} \,/\, \mathrm{C_5H_8O_2^-}\ (100\,\mathrm{amu}) \quad (4.28)$$

$$\rightarrow \mathrm{C_4H_4O_2^-} \,/\, \mathrm{C_5H_8O^-}\ (84\,\mathrm{amu}) \quad (4.29)$$

$$\rightarrow \mathrm{C_4H_6O^-}\ (70\,\mathrm{amu}) \quad (4.30)$$

All these radical anions may have a cyclic furan-like structure (figure 4.30) that can be formed from the parent ion by abstraction of all acetate groups. It is remarkable that electrons below 0.5 eV are able to induce this manifold bond-breaking reactions affecting the whole ring system.
On the other hand the group of heavier fragments (113, 119, 154, 161, 215 amu) occurs only around 2 eV and is created through abstraction of single exocyclic

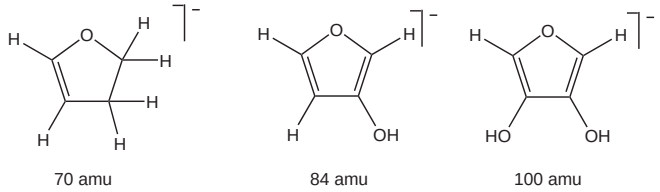

Figure 4.30: Possible molecular structures for the fragments anions at 70, 84 and 100 amu, respectively, which are generated by excission of all exocyclic groups.

species. The heaviest fragment ion was observed at 215 amu (not shown here) and is due to an abstraction of an acetic acid molecule and an acetyl radical (figure 4.31). All other ions can be created in a similar way by additional abstraction of the exocyclic groups.

4.2.3 Comparison with THF

A frequently used surrogate for 2-deoxy-D-ribose in DNA is tetrahydrofuran (THF) [88, 89, 90] as it possesses the heterocyclic ring structure of the furanose sugar, but no hydroxyl groups. However, THF is only very weakly subject

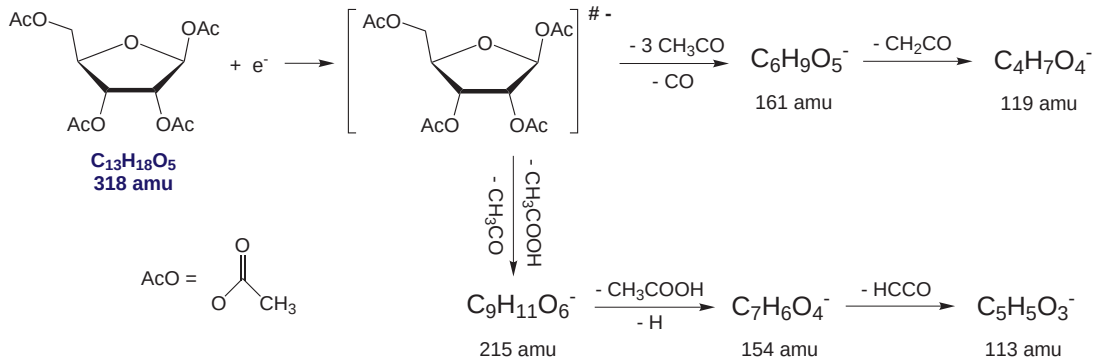

Figure 4.31: Fragmentation of the transient negative ion TAR^- by abstraction of acetic acid, the acetyl radical, carbon monoxide, ketene and the ketenyl radical resulting in fragment anions at 113, 119, 154, 161 and 215 amu, respectively.

to dissociative electron attachment and only at energies around 8 eV. Figure 4.32 displays the ion yield of HC_2O^- (41 amu), which is the only fragment ion that could be detected in dissociative electron attachment to THF in the gas phase in our laboratory [91, 92]. It shows a single peak at 7.8 eV that is due to a core

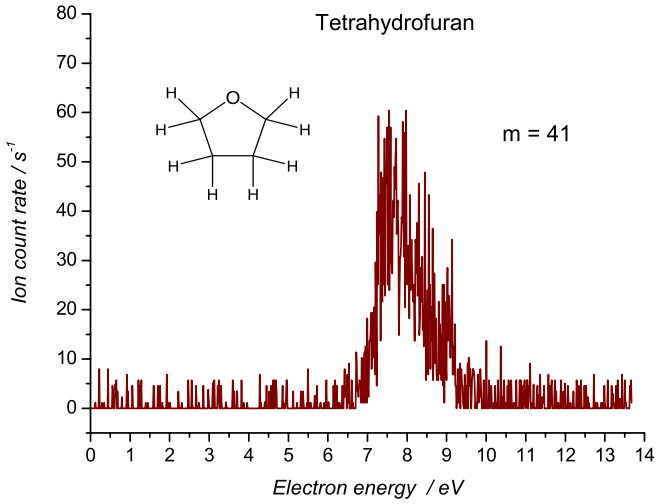

Figure 4.32: Ion yield of HC_2O^- (41 amu), which is the only fragment ion that could be detected in DEA to THF in the gas phase in our laboratory [91].

excited resonance what was confirmed by R-matrix calculations [93]. The count rates are very low indicating that THF is a weak electron scavenger that undergoes DEA only via core-excited resonances. A comparison of D-ribose and TAR

with THF shows that the appearance of threshold signals and consequently very complex fragmentation reactions is bound to the presence of polar groups that are connected to the carbon ring, no matter if these are free hydroxyl groups or acetyl groups. This supports the picture that decomposition proceeds via dipole bound states. In DNA and RNA the sugar is bound to two phosphate groups and one nucleobase, which can be considered as polar functional groups suggesting that the characteristic signals of the central sugar ring is also preserved in these systems.

4.2.4 Conclusions

Tetraacetyl-D-ribose is decomposed through dissociative electron attachment within three energy regions: (1) close to zero eV similar to the free sugars, (2) between 2 and 3 eV via π^* shape resonances that are located outside the ring on the acetate groups, (3) a core excited resonance at 7 - 11 eV. The dominant fragment anion is the acetate anion CH_3COO^-, which is formed within all three energy regions. A series of heavy fragment ions appears exclusively from the π^* shape resonances at 2 - 3 eV. A further series of light fragments (70, 84, 100 amu) is due to a loss of all exocyclic groups and is generated at threshold and through the core excited resonance. The peak shapes and masses of this group of ions are reminiscent to the signals observed in free D-ribose.

The five-membered sugar ring connected to polar functional groups leads to the same characteristic signals close to zero eV like the isolated sugars thus enabling the initial formation of a dipole-bound state. The presence of adjacent moieties additionally leads to π^* shape resonances in the low energy regime that are also expected if phosphate groups are present instead of acetate groups.

4.3 The phosphate moiety: DEA to phosphate esters

4.3.1 Previous investigations

The phosphate group is the central moiety in the DNA backbone that connects two adjacent 2-deoxy-D-ribose units of the respective nucleosides (figure 4.33). A strand break presumably occurs at a P-O or a C-OP bond. In the discussions of low energy electron induced DNA damage a direct electron attachment of the phosphate group was barely considered. Due to experimental difficulties an active role of the phosphate group was first investigated by theory. DFT calculations on a sugar-phosphate-sugar unit [16] suggested that electrons near zero eV are able to induce strand breaks via the C3-O and C5-O bond, respectively. On the other hand, a subsequent theoretical study [20] (considering explicitly metastable states rather than stable anions as in reference [16]) found that only electrons with an energy exceeding 2 eV are able to attach directly to a π^* orbital of the phosphate group. A very recent investigation of 5'-thymidine-phosphate [48], however, found that below 2 eV a transient negative ion could be formed and that a localisation of the extra electron on the phosphate more likely leads to a strand break than does the initial localisation on a nucleobase. No gas phase experiments had been performed to elucidate that question, the only experimental investigations on the phosphate group have been conducted in the condensed phase using electrons above 4 eV [94]. Very recently electron stimulated desorption (ESD) of H^-, O^- and OH^- from NaH_2PO_4 was reported [94] with the respective maxima at 8.8, 8.0 and 7.3 eV. This confirms an earlier study on self-assembled monolayers of single and double stranded DNA prepared from a 40mer oligonucleotide [11], where ESD of OH^- was observed at 6.7 eV that was ascribed to direct electron attachment to the phosphate group. It is interesting to note that the nature of the counter ion of the phosphate group, i.e. either Na^+ as in NaH_2PO_4 [94]

or H^+ as in the SAMs [11], does not influence strongly the electron attachment process and hence OH^- formation. Low energy (4 - 15 eV) electron interaction with shorter oligonucleotides (GCAT) [95, 96] employing high-performance liquid chromatography (HPLC) for analysis of products revealed that preferentially the C-O bond is broken than the P-O bond.

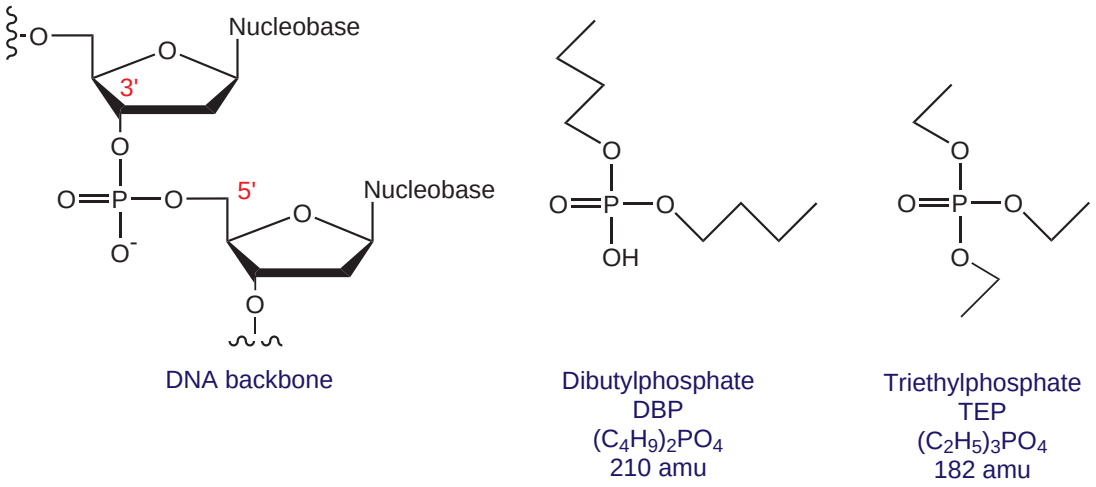

Figure 4.33: Schematic structure of the phosphate group coupled within the DNA backbone compared with the structure of DBP.

To elucidate the intrinsic properties of the phosphate group - especially at electron energies down to few meV - the phosphodiester dibutylphosphate (DBP, figure 4.33) and the phosphotriester triethylphosphate (TEP) are studied here in the gas phase. The measurements have been performed in collaboration with Constanze König within her diploma thesis and the spectra are already reported in references [97, 98].

4.3.2 Fragmentation pathways in DBP

The most dominant fragment anions are created by a single O-H or P-O bond cleavage, respectively, resulting in formation of $(DBP\text{-}H)^-$ and OH^-:

$$e^- + \mathrm{DBP} \quad \rightarrow \quad (\mathrm{DBP} - \mathrm{H})^- \,(209\,\mathrm{amu}) + \mathrm{H} \tag{4.31}$$

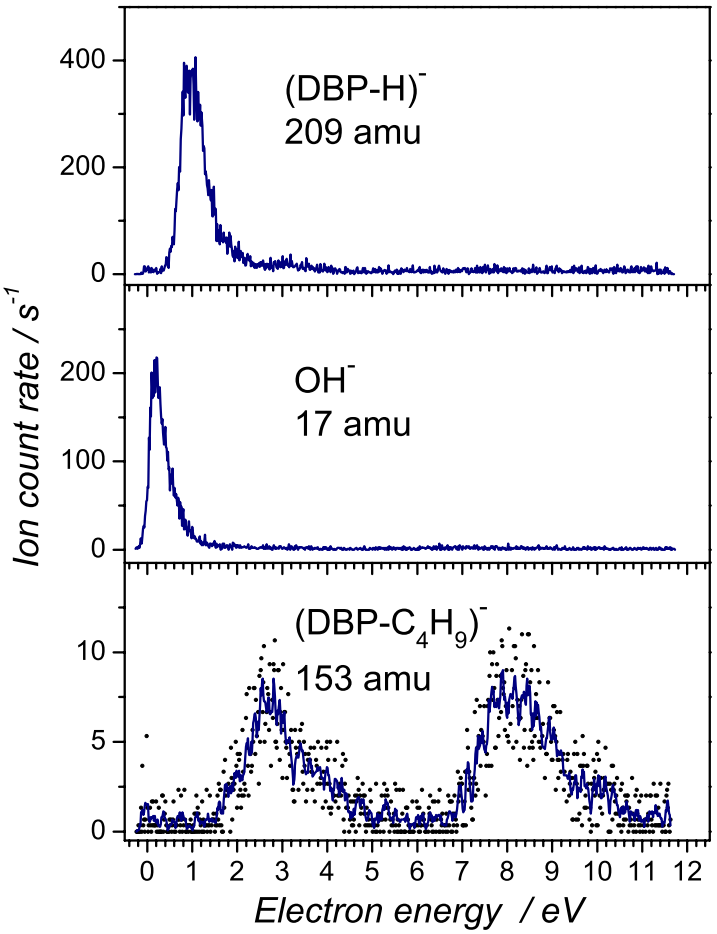

Figure 4.34: Ion yields of the main fragmentation products in DBP that are due to a single bond breaking.

$$\rightarrow \quad OH^- \,(17\,\text{amu}) + (C_4H_9)_2PO_3 \tag{4.32}$$

The H abstraction leading to $(DBP\text{-}H)^-$ proceeds most likely from the OH group, since this reaction was not observed in TEP. As can be seen in figure 4.34 at least two resonances contribute to the signal located around 1 eV. A third contribution arises at 3.1 eV.

OH^- anion formation is peaking at 0.2 eV. With the electron affinity of OH (1.83 eV [57]) and assuming that the reaction proceeds right at the thermodynamic threshold, a bond dissociation energy of the P-OH bond can be derived to

be approximately 2.0 eV.

A third anion that is produced by a single bond cleavage is the $(\mathrm{DBP\text{-}C_4H_9})^-$ anion (figure 4.34), which is due to loss of an entire butyl group:

$$e^- + \mathrm{DBP} \quad \rightarrow \quad (\mathrm{DBP} - \mathrm{C_4H_9})^- \,(153\,\mathrm{amu}) + \mathrm{C_4H_9} \tag{4.33}$$

It is generated through two broad resonances located at 2 - 4 eV and 7 - 10 eV. If the same reaction takes place in DNA this corresponds to a direct single strand break by a C-OP bond breaking.

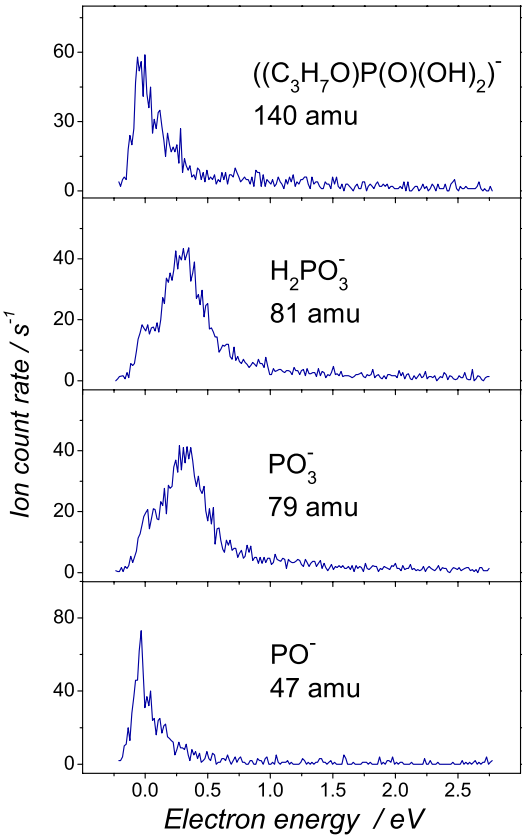

Figure 4.35: Fragment anions that are formed by multiple bond breaking subsequent to electron attachment to DBP.

The ion yields presented in figure 4.35 correspond to more complex reactions that are accompanied by an excission of the central phosphate group:

$$e^- + \mathrm{DBP} \quad \rightarrow \quad \mathrm{H_2PO_3^-}\,(81\,\mathrm{amu}) \tag{4.34}$$

$$\rightarrow \quad PO_3^- \ (79\,\text{amu}) \tag{4.35}$$

$$\rightarrow \quad PO^- \ (47\,\text{amu}) \tag{4.36}$$

These reactions proceed at energies as low as 0 - 0.5 eV via two overlapping resonances at 0.3 and 0 eV, respectively. Thermodynamic values like heats of formation are hardly explored for the present systems. However, the electron affinities of PO_3 and PO are known to be 4.95 [99] and 1.09 eV [100], respectively. This could be the driving force for the reactions 4.34 - 4.36. For the formation of the 140 amu ion also multiple bond breaking is necessary, a possible structure is $[(C_3H_7O)P(O)(OH)_2]^-$.

4.3.3 Fragmentation pathways in TEP

To investigate the influence of the free hydroxyl group on the observed reactions DEA experiments on triethylphosphate (TEP, figure 4.33) have been performed. Due to the high vapour pressure of TEP the sample was introduced into the HV chamber through a leak valve, hence the ion count rates shown in figure 4.36 cannot be directly compared with the spectra of DBP.

Neither the parent ion after loss of hydrogen ($(\text{TEP-H})^-$) nor OH^- could be observed in this experiment confirming that in DBP hydrogen and OH^- abstraction take place at the OH site. Similar to DBP PO_3^- and $H_2PO_3^-$ are detected close to zero eV (in figure 4.36). But PO_3^- additionally appears at higher energies around 8 eV. At almost the same energy but with a somewhat broader signal peaking at 7.5 eV a further ion was recorded at 137 amu that is due to an abstraction of an ethoxy radical:

$$e^- + \text{TEP} \quad \rightarrow \quad (C_2H_5)_2OPO^- \ (137\,\text{amu}) + OC_2H_5 \tag{4.37}$$

Thus the higher energy signal in TEP leads to both C-O and P-O bond breaking, both reactions corresponding to strand breaks in DNA. In DBP and TEP electrons having an energy of 7 - 9 eV induce a loss of a single alkyl group, i.e.,

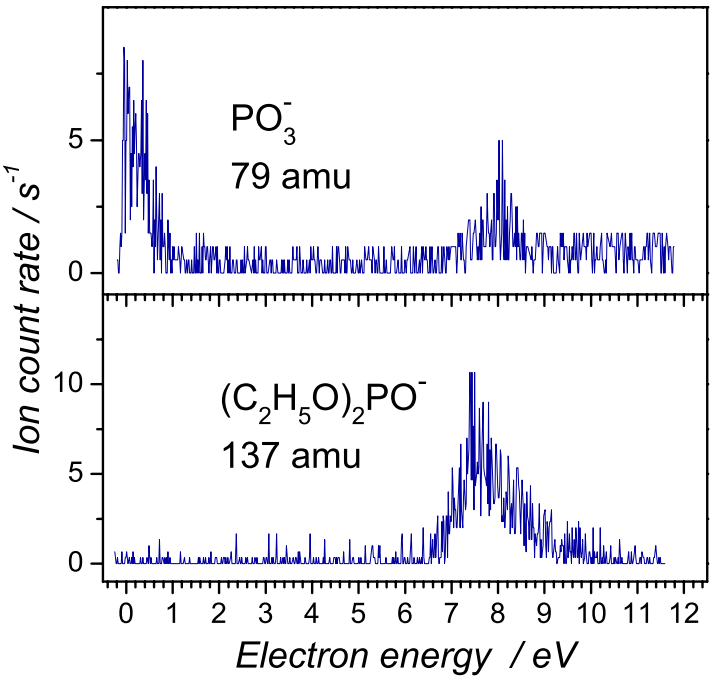

Figure 4.36: Fragment anions generated upon electron attachment to TEP.

C_4H_9 and OC_2H_5. In saturated hydrocarbons low energy resonances are usually not present in contrast to core excited resonances that are often observed in the energy region 6 - 9 eV. Therefore the low energy features in the DEA spectra of DBP and TEP are characterised as shape resonances with the extra electron occupying a π^* orbital of the phosphate group whereas the high energy signals are associated with an electronic excitation in the alkyl chain.

Zheng et al. [96] reported that phosphodiester bond cleavage occurs preferentially at the C-O bond rather than the P-O bond with maxima at 6 and 10 eV. Their experiments indicated that charge transfer from the nucleobases to the backbone with subsequent bond cleavage must contribute to these reactions. However, the gas phase experiments on DBP and TEP show that also core excited resonances in the vicinity of the phosphate group may contribute to phosphodiester bond cleavage. Furthermore electron attachment and dissociation was shown to be

operative already at low energy clearly below 3 eV.

4.3.4 Conclusions

Electron attachment to the phosphate group was investigated using the model substance dibutylphosphate. The parent ion after loss of hydrogen was observed within a resonant feature peaking at 1 eV; a formation of OH^- already occurs at 0.2 eV. A C-O bond cleavage representing the loss of a whole butyl group proceeds within two broad resonances at 2 - 4 eV and 7 - 10 eV. Very close to zero eV the central phosphate group is excised resulting in $H_2PO_3^-$, PO_3^- and PO^- formation. These results indicate an effective decomposition of dibutylphosphate by electron capture at subexcitation energies (< 4 eV). For the phosphate group coupled within DNA the observed reactions correspond to a direct strand break. These results confirm previous theoretical studies that predicted electron attachment to the phosphate group at energies down to zero eV [16].

4.4 DEA to labile biomolecules using LIAD

First results are presented for DEA of biomolecules that are desorbed by means of LIAD. The experimental arrangement was first tested and optimised with 5-bromouracil, since it is a stable molecule that produces Br^- upon electron capture with very high cross section [101]. To ensure that also thermal labile molecules can be transported intact into the gas phase the nucleoside thymidine was investigated. DEA of thymidine was studied before [14, 15], however, it turned out that the molecules are decomposed in the course of sublimation at elevated temperatures [15]. Finally, first results are presented on ribose-5-phosphate that have not been reported before.

4.4.1 Optimisation with 5-bromouracil

The complete setup shown in figure 3.2 was optimised using 5-bromouracil (BrU, figure 4.37) as it is known to efficiently capture 0 eV electrons [101] forming the parent ion as well as Br^- and the parent ion after loss of bromine (U^-):

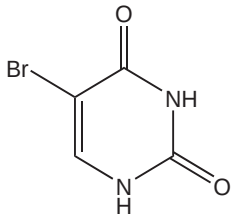

5-bromouracil
$C_4H_3O_2N_2Br$
^{79}BrU (189 amu)
^{81}BrU (191 amu)

Figure 4.37: Molecular structure of 5-bromouracil.

$$e^-(0eV) + \mathrm{BrU} \rightarrow \mathrm{BrU}^- \,(189/191\,\mathrm{amu}) \quad (4.38)$$

$$\rightarrow \mathrm{U}^- \,(110\,\mathrm{amu}) + \mathrm{Br} \quad (4.39)$$

$$\rightarrow \mathrm{Br}^- \,(79/81\,\mathrm{amu}) + \mathrm{U}^- \quad (4.40)$$

Br^- is generated with a cross section of $\approx 6{\times}10^{-14}\,\mathrm{cm}^2$ [101], which is in the same order of magnitude like SF_6^- production from SF_6.

In figure 4.38 negative ion mass spectra are displayed of the background (upper panel) and the desorbed 5-bromouracil (lower panel). The electron energy was fixed at 0 eV and the calibration gas SF_6 was present showing signals for SF_6^- and SF_5^-. The repetition rate of the laser was set to 15 Hz at

an energy of 3 mJ/pulse; approximately 7000 shots were collected from different spots. When the laser of the LIAD source was switched on the ions BrU^-, U^- and Br^- clearly appeared in the mass spectrum. The natural abundance of Br isotopes (50.7 % for ^{79}Br and 49.3 % for ^{81}Br) leads to characteristic double peaks for all bromine containing anions. The relative intensities correspond to the cross sections reported in [101].

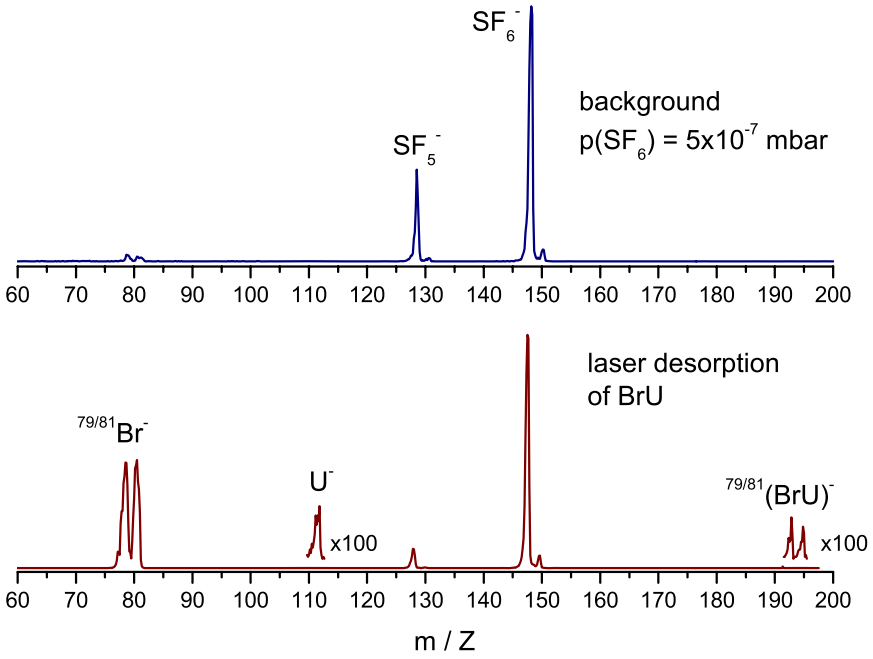

Figure 4.38: Negative ion mass spectra at 0 eV electron energy with resolution of about 0.8 eV. In the upper panel a background spectrum is shown with the calibration gas SF_6. For the lower mass spectrum the laser of the LIAD source was switched on resulting in desorption of BrU and production of BrU^-, U^- and Br^-. SF_6 produces SF_6^- (146 amu) and SF_5^- (127 amu); clearly visible are the characteristic isotope patterns of Br (50.7 % for ^{79}Br and 49.3 % for ^{81}Br) and S (4 % for ^{34}S and 95 % for ^{32}S).

To characterise the stability and the time dependence of a signal that is due to laser irradiation of a single spot on the Ti foil, the Br^- signal was recorded over the time using 15 Hz repetition rate and 3 mJ/pulse (Figure 4.39). The signal can be maintained over a period of more than 600 s. The ion count rate is even increasing what is most likely due to constant ablation of titanium leading to

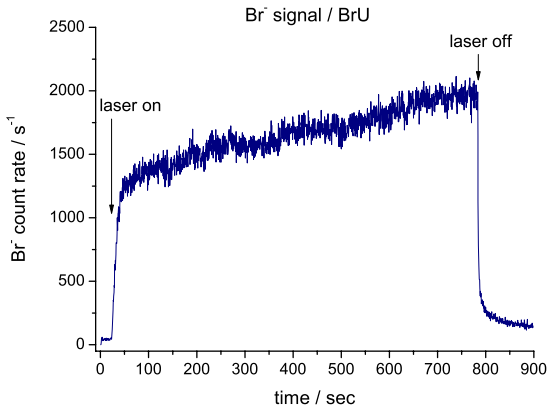

Figure 4.39: Time dependence of the Br- signal that is due to laser desorption of BrU from a single spot. The increase of signal is ascribed to continuous ablation of titanium from the backside of the foil resulting in stronger Br^- signal.

a thinner foil. When the laser is switched off the signal decreases immediately indicating that the observed signal is indeed a result of laser desorbed sample molecules. Nevertheless a weak Br^- signal is still observed in the background. This shows that in DEA measurements energy scans can be performed with a scan time of about 10 min while irradiating a single sample spot. Longer irradiation on a single spot should be avoided in order to prevent a strong reduction of the metal thickness and hence risk to heat the molecules on the surface by laser irradiation.

4.4.2 Thymidine

The sugar 2-deoxy-D-ribose in its furanose form is connected to the nucleobase thymine at the anomeric centre to form the nucleoside thymidine (Td; figure 4.40). It is so far the largest building block of the DNA that has been studied in the gas phase with respect to DEA [14, 15]. The parent ion after loss of hydrogen ($[Td\text{-}H]^-$) could be detected in DEA, but the most abundant fragment ion is generated by abstraction of the thymine unit (T) resulting in the closed shell anion of dehydrogenated thymine ($[T\text{-}H]^-$) [14, 15]. The ion yield curve of $[T\text{-}H]^-$ created from Td exhibits two main signals, one at 2 - 4 eV, and a second

broad peak at 5.5 - 9 eV [15] (figure 4.41). However, the first peak was previously observed in the ion yield curve of $[T\text{-}H]^-$ generated from isolated thymine [102, 22] with the same characteristic peak shape. Furthermore the first resonance is subject to a pronounced temperature dependence, therefore it was concluded in reference [15] that the resonance at 2 - 4 eV is due to thermal decomposition of thymidine that leads to bond cleavage of the N-glycosidic N-C bond and subsequently to thymine formation by hydrogen capture. Nevertheless the second peak at 5.5 - 9 eV was not observed before and is thus due to non-decomposed thymidine. Therefore the ion yield curve of $[T\text{-}H]^-$/Td is used here to evaluate if the samples in LIAD are desorbed intact and by a non-thermal mechanism.

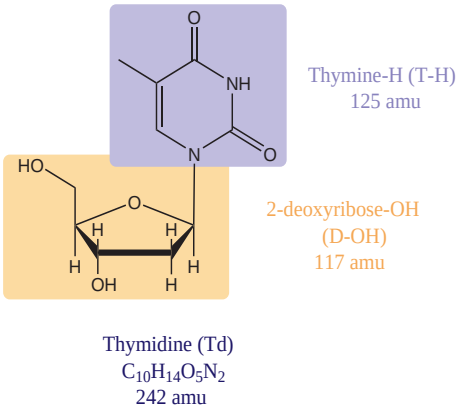

Figure 4.40: Molecular structure of Thymidine, that is composed of 2-deoxy-D-ribose and Thymine.

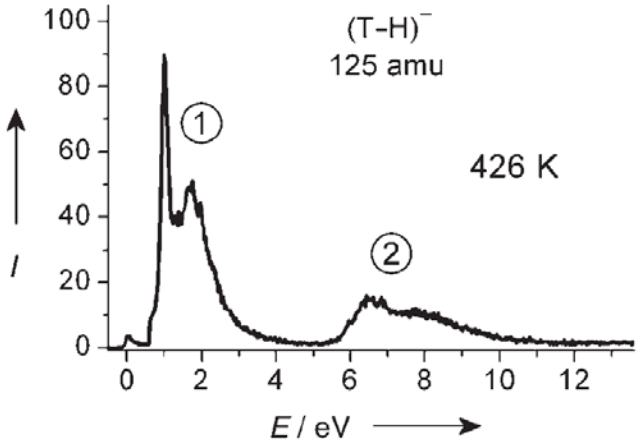

Figure 4.41: Ion yield of $(T\text{-}H)^-$ created through DEA to the nucleoside thymidine, which is thermally evaporated at 426 K. Taken from [15].

The DEA spectrum of $[T\text{-}H]^-$/Td that was recorded using LIAD is shown in figure 4.42. The count rates are very low due to the low cross sections (1.5×10^{-21} m^2 for

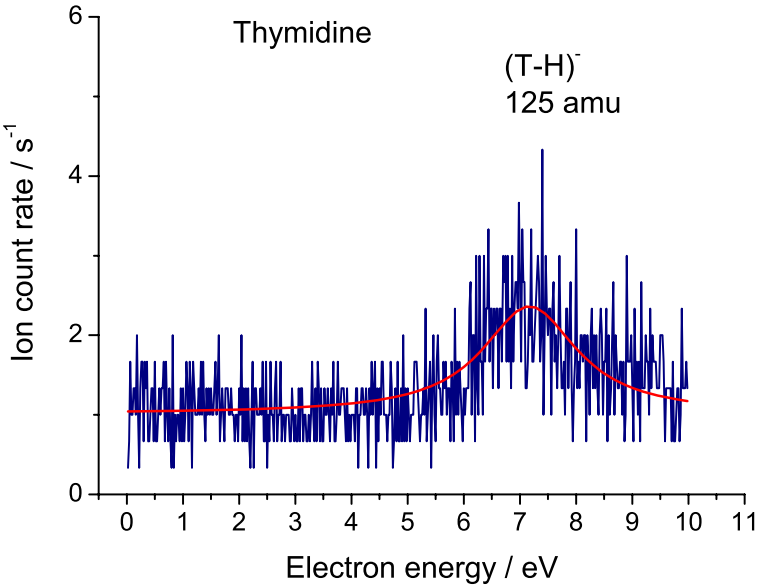

Figure 4.42: Ion yield of $(T\text{-}H)^-$ created from thymidine, which is desorbed by LIAD. The lack of a signal at lower energies confirms that no thermal decomposition occurs.

$[T\text{-}H]^-$ formation), nevertheless it is clear that ion formation proceeds exclusively at higher energies between 6 and 10 eV. No signal is detected at lower energies confirming that no decomposition takes place. Further fragment ions generated after electron attachment to thymidine are $[Td\text{-}H]^-$ and $[D\text{-}2H]^-$ [15], however, with clearly lower cross sections than for $[T\text{-}H]^-$ formation. Since $[T\text{-}H]^-$ was recorded right at the detection limit in the present experiment no other fragment ion could be observed here from thymidine.

4.4.3 D-ribose-5-phosphate

A strand break in DNA occurs finally at the phosphate sugar linkage. Model compounds of the single sugar and phosphate units have been extensively studied in the present work indicating that direct electron attachment to the backbone with subsequent bond breaking proceeds already at very low energies. However, a more comprehensive picture of the molecular mechanisms of strand break formation by electron attachment to the DNA backbone is only possible if a complete

phosphate-sugar compound is investigated. For this purpose DEA of D-ribose-5-

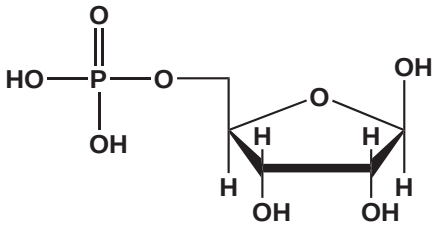

D-ribose-5-phosphate
RP
$C_5H_{11}O_8P$
230 amu

Figure 4.43: Molecular structure of D-ribose-5-phosphate.

phosphate (RP, figure 4.43) has been studied. The results are complemented by experiments on metastable decay of deprotonated RP.

DEA to D-ribose-5-phosphate

The structure of the Barium salt of D-ribose-5-phosphate was determined by x-ray crystallography to be a furanose ring [103] as it is shown in figure 4.43.
As it is apparent from the DEA spectrum of thymidine (figure 4.42) the sensitivity of the present technique is still very poor what is so far the main disadvantage. Anyhow two main product anions could be clearly identified at 97 and 149 amu in DEA to D-ribose-5-phosphate that are shown in figure 4.44. They are associated with the following dissociation reactions:

$$e^- + RP\,(230\,amu) \rightarrow (C_5H_9O_5)^-\,(149\,\text{amu}) + H_2PO_3 \quad (4.41)$$

$$\rightarrow (H_2PO_4)^-\,(97\,\text{amu}) + C_5H_9O_4 \quad (4.42)$$

The transient negative ion $RP^{-\#}$ is thus generated near 0 eV and dissociates subsequently either along the P-O or the C-O bond with the negative charge remaining on the sugar or the phosphate group, respectively (figure 4.45). Both

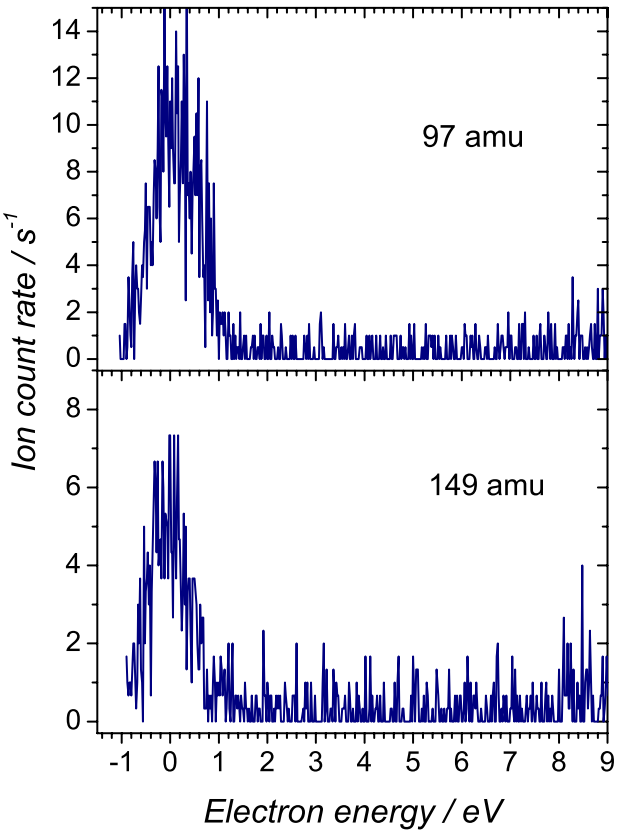

Figure 4.44: Ion yields of the fragments at 149 amu and 97 amu subsequent to electron attachment to D-ribose-5-phosphate, which was transported into the gas phase by LIAD.

reactions correspond to a strand break in RNA or DNA. It should be noted that in the free sugar D-ribose no fragment ion at 149 amu was observed indicating that the signals are not due to a decomposition of RP prior to electron attachment. The electron affinity of H_2PO_4 is remarkably high with 4.57 eV [104] that makes the reaction accessible already at zero eV. In the phosphate esters discussed in chapter 4.3 no $H_2PO_4^-$ was observed, since the oxygen atoms are blocked by alkyl groups. On the other hand the C-O bond breaking in RP accompanied by an abstraction of the sugar moiety corresponds to the abstraction of a butyl group in DBP creating $(DBP\text{-}C_4H_9)^-$. This reaction is accessible in RP at lower energies than in DBP due to a presumably positive lectron affinity of RP and the high

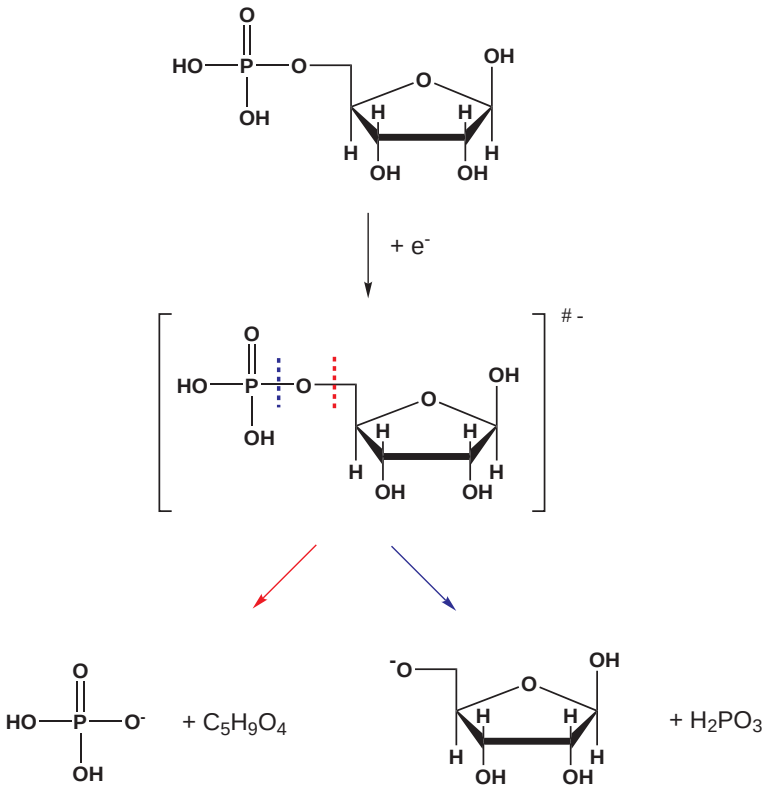

Figure 4.45: Reaction scheme of the decomposition of the TNI $RP^{-\#}$ resulting in the formation of $H_2PO_4^-$ and $C_5H_9O_5^-$.

electron affinity of H_2PO_4.

The extra electron might be captured into the virtual orbitals of the phosphate group or alternatively by the sugar unit in a similar mechanism like in free D-ribose and acetylated D-ribose. Both mechanisms may be simultaneously possible leading to the two different decomposition products, *viz.* $C_5H_9O_5^-$ and $H_2PO_4^-$.

Metastable decay of deprotonated D-ribose-5-phosphate

The metastable decomposition of $(RP\text{-}H)^-$ was measured by means of MALDI-PSD and is shown in figure 4.46. The fragmentation products are due to:

$$(RP-H)^- \,(229\,amu) \rightarrow (H_2PO_4C_5H_7O_3)^- \,(211\,\text{amu}) + H_2O \qquad (4.43)$$

$$\rightarrow (H_2PO_4C_5H_5O_2)^- \,(193\,\text{amu}) + 2\,H_2O \qquad (4.44)$$

$$\rightarrow \quad (H_2PO_4C_4H_7O_3)^- \,(169\,\text{amu}) + CH_2O \qquad (4.45)$$

$$\rightarrow \quad (H_2PO_4C_4H_5O_2)^- \,(139\,\text{amu}) + 2\,CH_2O \qquad (4.46)$$

$$\rightarrow \quad (H_2PO_4)^- \,(97\,\text{amu}) + C_5H_9O_4 \qquad (4.47)$$

$$\rightarrow \quad (PO_3)^- \,(79\,\text{amu}) + C_5H_9O_4 + H_2O \qquad (4.48)$$

The dominant fragment anion is $H_2PO_4^-$ at 97 amu similar to the DEA spectra.

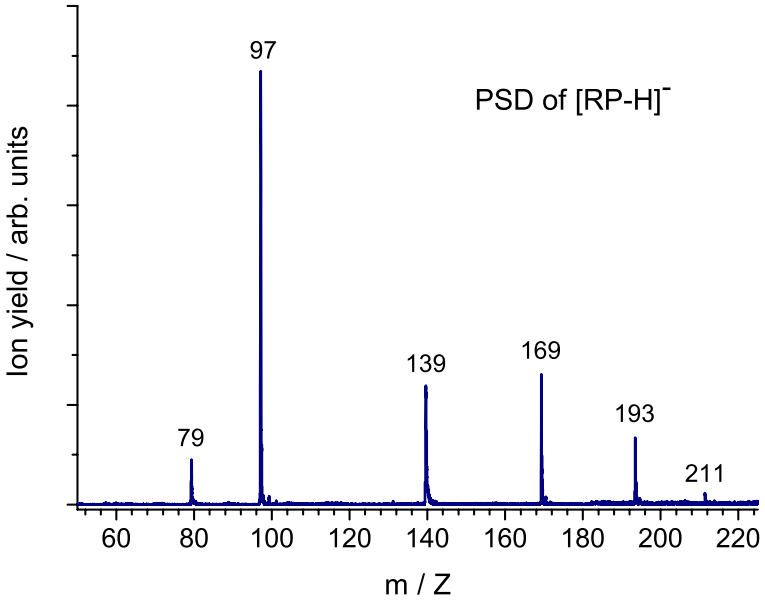

Figure 4.46: Metastable decay of $(RP\text{-}H)^-$ as measured in MALDI-PSD.

$(RP\text{-}H)^-$ decomposes with the same characteristic fragmentation pattern like the pure sugars, i.e. by abstraction of one or two water and formaldehyde molecules, respectively, from the D-ribose unit. However, no peak is observed at 149 amu suggesting that the initial charge state is considerably different in $(RP\text{-}H)^-$ and the TNI $RP^{-\#}$. Deprotonation occurs most likely at the phosphate group and the negative charge remains always on the fragment containing the phosphate group. On the other hand in free-electron attachment of RP the extra electron may be localised on the sugar moiety leading to P-O bond breaking with the negative charge remaining on the sugar.

4.4.4 Future prospects

The main disadvantage of the application of LIAD in DEA is the poor sensitivity due to low concentration of sample molecules. Anyway, the present results are only the first steps and show that the technique is basically working. There are different possibilities for improvement: (a) The use of a free laser beam instead of a fibre optic allows to apply more laser power per pulse. It was shown previously [58, 105] that the laser power is a crucial parameter. Moreover with higher laser power the irradiated spot can also be enlarged leaving the power per area unchanged that finally leads to larger amounts of desorbed molecules. (b) The electron gun and also the ion detection can be pulsed together with the laser pulse. Hence the ionisation and detection occurs only during the actual desorption of neutral molecules. This may improve the signal to noise ratio substantially since the laser pulse width (and hence the time of desorption) is very short (2 - 6 ns) and the repetition rate is low (15 Hz). (c) The use of a time-of-flight (TOF) mass spectrometer is more suitable for a pulsed desorption source. The ion detection is much faster and also more sensitive.

With the LIAD source it will be possible to measure DEA of whole nucleotides, what will help to understand where the extra charge is initially localised. Experiments with short oligonucleotides could shed some light on the base and sequence dependence of fragmentation reactions.

4.4.5 Conclusions

Laser-induced acoustic desorption was used to transport thermally labile biomolecules into the gas phase. 5-bromouracil was successfully desorbed followed by low-energy electron irradiation and detection of negative ions. A gentle desorption of intact molecules was demonstrated using thymidine. The ion yield curve of $[\text{Thymine-H}]^-$, which is generated by N-glycosidic bond cleavage in thymidine, exhibits a single maximum around 7 eV. The low-energy resonance at 1.2 eV that

is observed in isolated thymine [102, 22] is completely suppressed in thymidine. The thermal decomposition that was observed previously in DEA to thermally heated thymidine [15], is not observed using LIAD.

Dissociative electron attachment to ribose-5-phosphate was studied applying laser-induced acoustic desorption. Electron attachment close to zero eV was observed resulting in the formation of $H_2PO_4^-$ and (Ribose-H)$^-$, which are created by a C-O and P-O bond cleavage, respectively. Both reactions represent a strand break in DNA or RNA at very low electron energies confirming the results on smaller subunits discussed in the preceding chapters.

The method presented here can be applied in the future to investigate dissociative electron attachment to more complex molecules such as mono- or short oligonucleotides.

4.5 DEA to hexafluoroacetone azine: Energy-selective formation of CN^-

In the preceding chapters it was shown that low energy electrons induce specific and also highly selective reactions in more or less complex biomolecules. On the one hand this helps to understand the nascent mechanisms in radiation damage to living cells, on the other hand it indicates that low energy electrons may be a means to control chemical reactions in a highly selective way. To explore low-energy-initiated reactions in more complex (though non-biological) molecules, DEA of hexafluoroacetone azine (HFAA) was investigated.

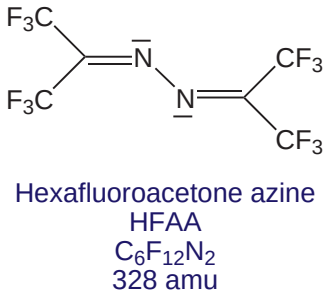

Figure 4.47: Molecular structure of Hexafluoroacetone azine.

HFAA is perfluorinated and possesses two CN groups, which are connected by an N-N bond (figure 4.47) and is hence expected to possess interesting properties with respect to anion formation via free-electron attachment.

4.5.1 Outline of fragmentation reactions

Figures 4.48 - 4.49 show that electron attachment to HFAA yields various fragment anions that arise from different resonances at energies ranging from 0 - 12 eV. The underlying reactions are:

$$e^- + \text{HFAA}\,(338\,\text{amu}) \rightarrow (CF_3)_2CN^-\,(164\,\text{amu}) + NC(CF_3)_2 \quad (4.49)$$

$$\rightarrow (CF_3)_2C^-\,(150\,\text{amu}) + N_2(CF_3)_2 \quad (4.50)$$

$$\rightarrow \quad CF_3^- \ (69\,\text{amu}) + CF_3CNNC(CF_3)_2 \qquad (4.51)$$

$$\rightarrow \quad CN^- \ (26\,\text{amu}) + C_2F_6 + NC(CF_3)_2 \qquad (4.52)$$

$$\rightarrow \quad F^- \ (19\,\text{amu}) + CF_2CF_3CNNC(CF_3)_2 \qquad (4.53)$$

All fragments with exception of CN^- can be generated by simple bond cleavages. For the excission of the cyanide anion multiple bond breaking and rearrangement of the neutral products is necessary.

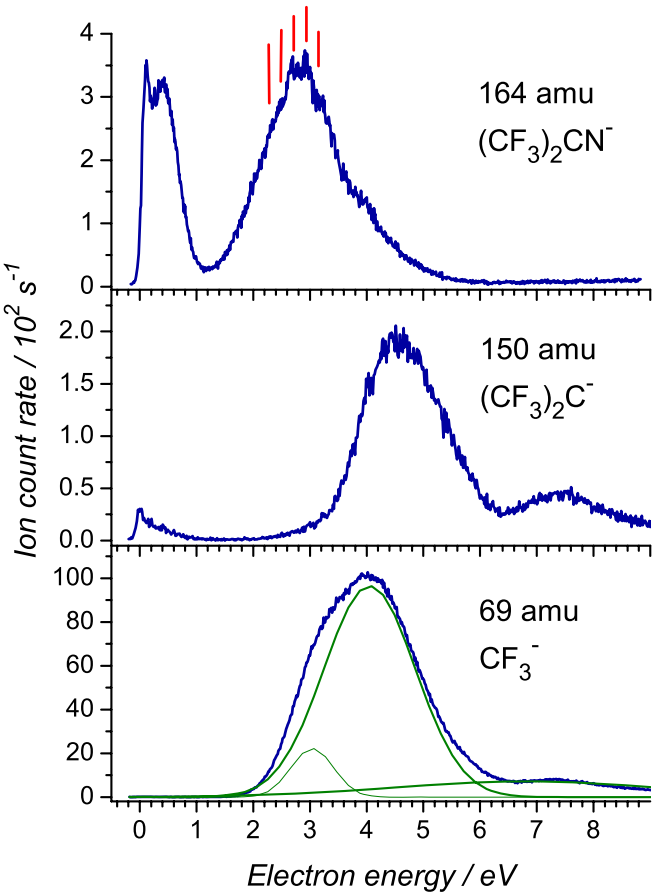

Figure 4.48: Ion yields of the fragments $(CF_3)_2CN^-$ (164 amu) with clearly reproducible vibrational structures indicated by red lines, $(CF_3)_2C^-$ (150 amu) and CF_3^- (69 amu).

The present experimental setup displayed in figure 3.1 (chapter 3.1 on page 30) only allows detection of fragment ions with a mass below 300 amu. Thus the parent ion $HFAA^-$ (328 amu) could not be detected. However, measurements performed by I. Martin and J. Langer on the cluster beam apparatus of our

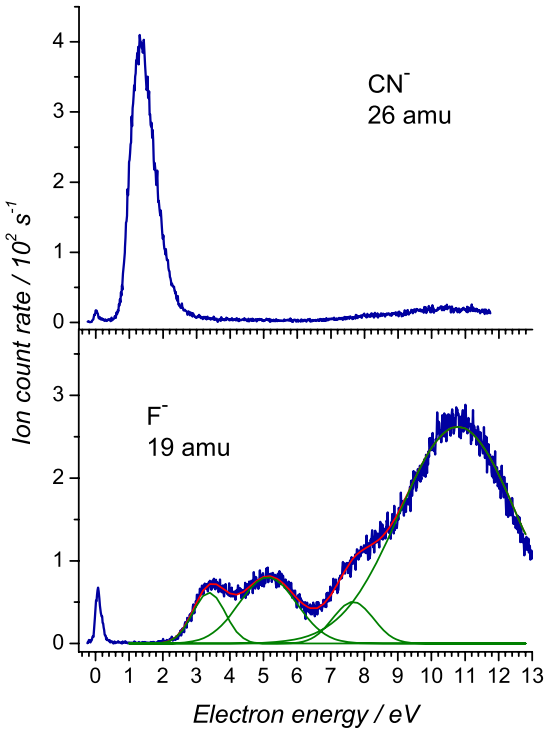

Figure 4.49: Ion yields of CN^- (26 amu) and F^- (19 amu). Only CN^- is formed from the resonance at 1.35 eV, it additionally appears weakly at 10 - 11 eV, where the F^- yield shows a pronounced maximum.

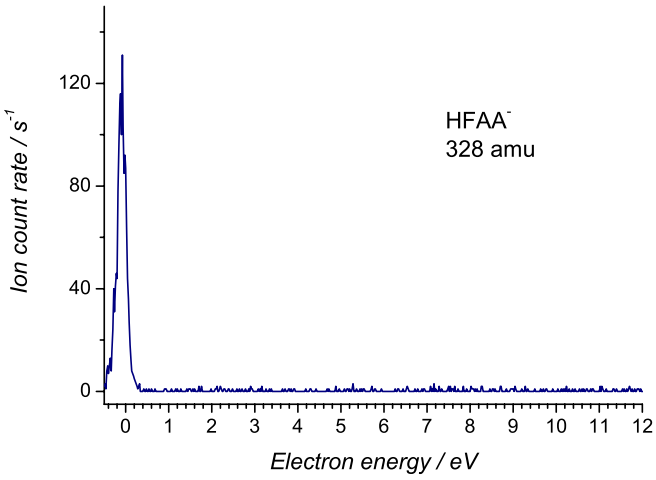

Figure 4.50: Ion yield of the parent ion $HFAA^-$, measured by I. Martin and J. Langer.

laboratory revealed a weak signal close to zero eV, that is due to the undissociated $HFAA^-$ (figure 4.50). The TNI created at zero eV hence possesses a lifetime of

at least 10 μs, which is the approximate flight time to the detector. Therefore the parent ion is metastable with respect to autodetachment and dissociation. The only dissociation reaction that is accessible close to zero eV (see below) is the symmetric cleavage of the N-N bond according to equation 4.49.

4.5.2 Negative ion states of HFAA

Ab initio calculations on HFAA at the MP2/cc-pVTZ level [106] revealed an adiabatic electron affinity of HFAA of 1.99 eV. Since the TNI $HFAA^{-\#}$ is generated at the geometry of the neutral the parent ion is vibrationally excited and the excess energy must be redistributed into other vibrational degrees of freedom to access the relaxed geometry of the anion.

Figure 4.51 shows the calculated ground state geometries of the neutral and anionic HFAA (MP2/cc-pVTZ). The view along the C2-N4-N5 plane (middle) indicates that an excess electron triggers a significant geometry change, i.e., the dihedral angle C2-N4-N5-C6 changes from 110° in the neutral to 180° in the anion. On the right-hand side the LUMO of the neutral and the SOMO of the anion is displayed. The SOMO possess a pronounced π^*_{CN} antibonding character, but a π^*_{NN} bonding character. This leads to an elongation of the C-N bond (128 pm to 132 pm) and a shortening of the N-N bond (134 pm to 132 pm). The resulting equal C-N and N-N bond lengths indicate that the excess electron becomes fully delocalised over the CNNC centre.

At energies below 1 eV exclusively $(CF_3)_2CN^-$ was observed since this is the only reaction that is thermodynamically accessible at low energies (see next section). The signal shows two distinct maxima at 0.1 eV and 0.4 eV. Weak threshold signals in the ion yield curves of other fragments are most likely due to hot band transitions or small amounts of impurities. Such signals can strongly contribute at threshold due to the reciprocal energy dependence of the DEA cross section. A further narrow resonance is observed at 1.35 eV, which exclusively leads to

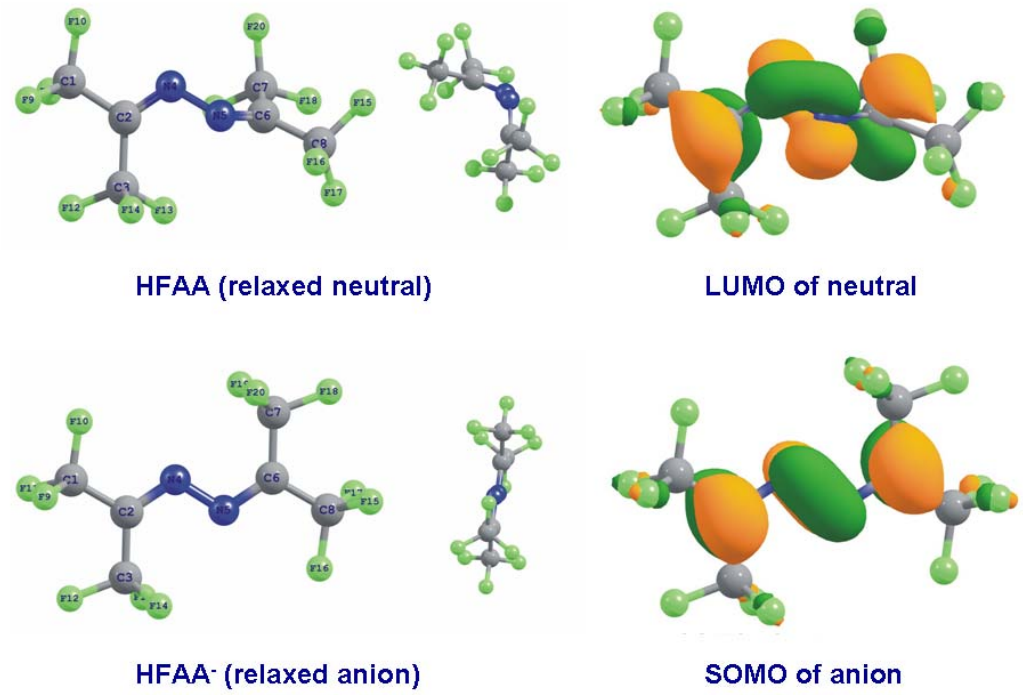

Figure 4.51: Geometries of the ground state neutral HFAA and the anion $HFAA^-$, optimised at MP2/cc-pVTZ level. The geometry change is visible along the C2-N4-N5 plane, shown in the middle. The right hand side displays the corresponding molecular orbitals, i.e. the LUMO of the neutral system and the first singly occupied molecular orbital (SOMO) of the anion in its relaxed geometry. The orbitals are plotted with a contour line spacing of 0.05 $Bohr^{-3/2}$. Calculations performed by I. Dabkowska [106].

formation of CN^-. No other fragment ion could be observed through this resonance. All fragment anions with exception of CN^- are generated within at least two overlapping resonances between 2 and 6 eV (figures 4.48 and 4.49).

At low energies exclusively shape resonances are expected. UV absorption spectra of non-fluorinated acetone azine [107] show a broad band at 6 eV that is assigned to the $\pi^* \leftarrow \pi$ transition. For fluorinated compounds it is expected in reference [107] that the HOMO - LUMO gap is even larger. Since core excited resonances occur close to the energy of the actual electronic excitation all features below 5 eV

in the DEA spectra of HFAA can be tentatively assigned to shape resonances. The resonances at 0.1 - 0.4 eV and 1.35 eV must then be due to a temporary occupation of the two π^* orbitals that are present in HFAA. For the symmetric N-N bond cleavage leading to $(CF_3)_2CN^-$ intramolecular vibrational redistribution takes place, representing vibrational predissociation.

The resonances at 2 - 6 eV are composed of at least two contributions that result in different dissociation products. This is visible in the broad signal in the ion yield curve of $(CF_3)_2CN^-$, which peaks at 2.8 eV exhibiting also a clear shoulder around 4 eV. Complementary the 4 eV resonance results predominantly in CF_3^-, which appears weaker through the lower energy resonance (figure 4.48). Decomposition into $(CF_3)_2C^-$ proceeds only through the higher energy resonance with a maximum at 4.6 eV.

By far the most dominant signal is CF_3^-. Its strong intensity suggests that the C-CF_3 antibonding σ^* orbital is directly populated by the extra electron, thus representing one or more $\sigma^*_{C-CF_3}$ shape resonances. The other signals at 2 - 6 eV may thus be due to shape resonances having σ^*_{N-N} or σ^*_{C-N} character, respectively.

At higher energies core excited resonances are observed. One is located at 7 - 8 eV and appears through $(CF_3)_2C^-$, CF_3^- and F^- formation. It may be attributed to a $\pi^* \leftarrow \pi$ transition. A second core excited resonance is located around 11 eV and results in strong formation of F^- and weakly in CN^-. It is most likely due to an excitation into a Rydberg-like orbital and is located in the ionisation continuum of the neutral molecule.

4.5.3 Fragment ions

$(CF_3)_2CN^-$

In figure 4.52 thermodynamic thresholds for $(CF_3)_2CN^-$ and CN^- formation according to MP2 calculations are shown. Experimental data on these systems

are barely available, therefore calculations have been performed by I. Dabkowska [106]. The appearance energy of $(CF_3)_2CN^-$ is close to zero eV, however, the calculations predict a threshold of 0.89 eV. The uncertainty of calculations is estimated to be below 0.5 eV, and thus the appearance of the 0.1 eV peak can only be explained if vibrationally excited molecules are involved.

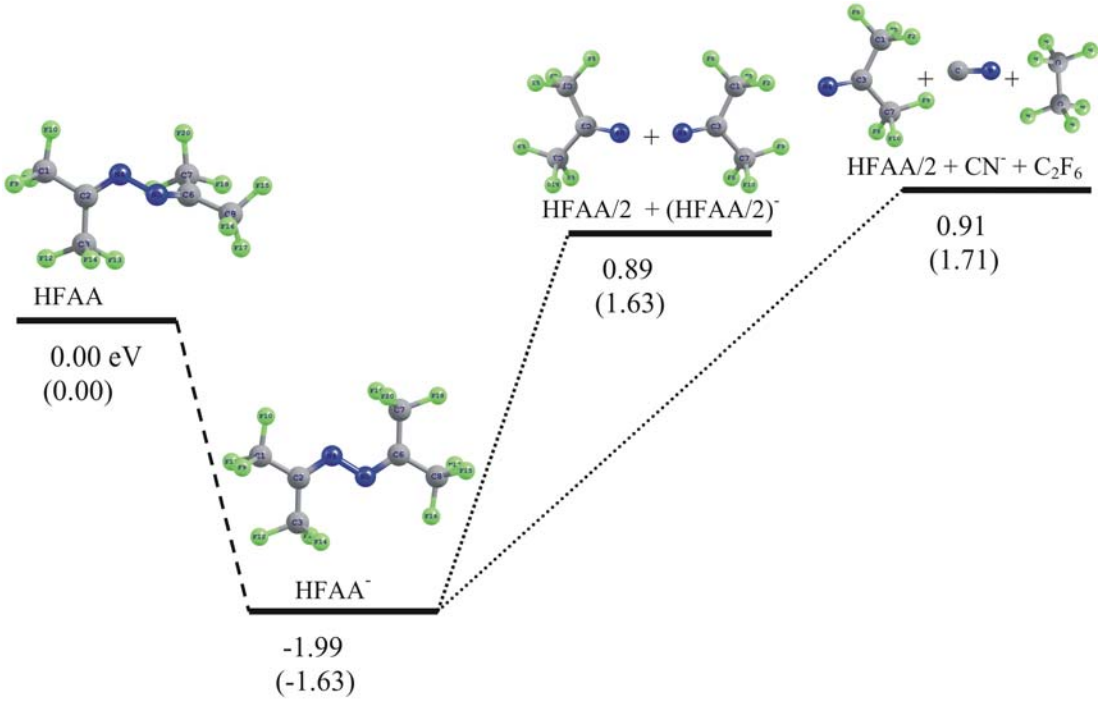

Figure 4.52: Relative energies of the neutral and anionic HFAA and threshold energies for the symmetric decomposition along the N-N bond and CN^- formation, calculated at the MP2/cc-pVTZ level (in brackets cc-pVDZ). Calculations performed by I. Dabkowska [106].

A closer inspection of the higher energy peak in the ion yield curve of $(CF_3)_2CN^-$ reveals a distinct and reproducible structure with a spacing of 220 ± 30 meV (figure 4.48). This can be attributed to vibrational excitation either in the transient anion or in one of the products. It was demonstrated previously for the case of DEA to CO_2 [108] that vibrational structures can be observed in the ion yield curve of O^-. The excess energy that is imparted by the electron may thus lead to a population of the vibrational excited levels of the TNI (v_i). After dissociation

the energy exceeding the thermodynamic threshold is dissipated into kinetic and internal energy (v_n) of the fragments:

$$e^- + CO_2 \rightarrow CO_2^{-\#}(v_i) \rightarrow O^- + CO(v_n) \tag{4.54}$$

It was possible in the experiment of Dressler and Allan [108] to modify the instrument such that both structures could be observed. In the electron transmission spectrum (ETS) the CO_2^- vibrations are visible. This is also possible in the O^- fragment ion yield in DEA, if the detection efficiency of the instrument is independent of the kinetic energy of the detected ion. A population of the vibrational levels of the product CO leads to lower translational energy of O^-. By setting the instrument to exclusive detection of ions possessing zero kinetic energy the vibrational structure of CO becomes visible on the O^- ion yield [108].
HFAA is much more complex possessing a large number of vibrational degrees of freedom. The observed spacing within the structure of the $(CF_3)_2CN^-$ yield is most likely due to C-N vibrations. The C=N stretching vibration in acetone azine was determined to be 201 meV [109] and the vibrational energy of the cyanide ion is 252 meV [110]. In the present situation the CN group is either coupled within the TNI or one of the fragments. The present experiment is operated close to the constant ion detection mode, hence the observed structures are ascribed to vibrations in the TNI rather than the fragments.

CN^-

For the formation of the cyanide anion two C-C and one N-N bond must be broken. For such a complex reaction the resonance energy is remarkably low. The cleavage of two C-C bonds would correspond to the formation of two CF_3 radicals. However, the thermodynamic threshold for this reaction is calculated to be 5.97 eV [106] and is thus too high for the reaction observed here. The only possibility is the formation of a suitable transition state that allows the simultaneous formation of a new C-C bond resulting in F_3CCF_3 generation and the excission of

fragment ion	resonance energies / eV	ΔH_0 / eV (see text)	cross section / $10^{-22}\,m^2$
$(CF_3)_2CN^-$	0.1, 0.4, **2.8**, 3.9	0.89	6
$(CF_3)_2C^-$	**4.5**, 7.4	3 - 4	2
CF_3^-	3.0, **4.0**, 7.3	2.1	150
CN^-	**1.4**, 10.5	0.91	6
F^-	3.4, 5.2, 7.6, **10.8**	1.6	6

Table 4.2: Observed energies of fragment anions, thermodynamic thresholds and estimated cross sections.

CN^-. Including C_2F_6 formation the thermodynamic threshold becomes 0.91 eV (figure 4.52), what is in agreement with the experimental appearance energy of 0.8 eV.

The cross section for CN^- formation is approximately $10^{-21}\,m^2$ (table 4.2) and thus larger than in other cyano compounds like acetonitrile [111] (CH_3CN) where the cyanide anion is generated only by a single C-CN bond cleavage. The cyano radical is a pseudohalogen with an electron affinity of 3.82 eV [110]. However, the low DEA cross sections in nitriles can be rationalised by comparison with halogenated molecules. DEA of the compounds CH_3I [112] and CH_3CN [111] producing I^- and CN^-, respectively, proceeds fundamentally different. In CH_3I the LUMO that is occupied by the extra electron possesses pronounced σ^* character leading to a direct dissociation along the repulsive potential curve with the whole excess energy transformed into kinetic energy of the fragments. In contrast to that CH_3CN captures an electron into a π^* orbital of the CN group and decomposition is only possible through vibrational predissociation leading to a cross section for CN^- formation that is six orders of magnitude lower than that for I^- generation out of CH_3I. Hence it is surprising that CN^- is formed out of HFAA through multiple bond breaking involving rearrangement at compara-

tively low energy and with high cross section. Similar processes are observed in biomolecules like DNA bases [113] and amino acids [114, 115, 116].
CN^- production from HFAA is remarkable energy selective as it arises from the resonance at 1.35 eV that is not observed in any other fragment ion yield.

$(CF_3)_2C^-$

A cleavage of the C=N double bond generates the $(CF_3)_2C^-$ ion according to equation 4.50. The same ion was observed in an early study of DEA to hexafluoroacetone [117], in which an electron affinity of ≈ 0.6 eV was estimated. The bond dissociation energy of the C=N bond is not known, but is expected to lie between 4 and 5 eV resulting in a thermodynamic threshold of at least 3.4 eV. Consequently $(CF_3)_2C^-$ is only observed through the higher energy resonance located at 4.5 eV and also the core excited resonance at 7.4 eV.

CF_3^-

The dominant product ion after electron attachment to HFAA is CF_3^-, with a maximum yield at 3.9 eV with a clear shoulder close to 3 eV. The electron affinity was determined to be 1.9 eV [118]. With a C-C bond dissociation energy of 4 eV the thermodynamic threshold is 2.1 eV, which is close to the experimental appearance energy.

F^-

Due to the well-established electron affinity of F (3.40 eV) and a typical C-F bond dissociation energy of 5.0 eV, the thermodynamic threshold of F^- formation is 1.6 eV. Anyhow the appearance energy (≈ 2.5 eV) is clearly higher. It is created through two broad, clearly separated resonances close to 3 and 5 eV, i.e., in the vicinity of the dominating resonances observed for the other fragment ions. Additionally a very broad and intense resonant feature is observed around 11 eV

that is also observed with weaker intensity in the CN^- yield. A clear shoulder is visible around 7.5 eV, which is attributed to the same core excited resonance that also leads to CF_3^- and $(CF_3)_2C^-$.

4.5.4 Conclusions

Hexafluoroacetone azine is efficiently decomposed by low energy electrons of various energies between 0 and 12 eV. The dominant fragment anion is CF_3^- with a cross section of $10^{-20}\,m^2$ peaking at 4.0 eV. Electrons with an energy of 1.35 eV *exclusively* produce CN^-, which is formed through multiple bond breaking and rearrangement of neutral products. At energies below 1 eV only a symmetric N-N bond cleavage is induced resulting in $(CF_3)_2CN^-$. The parent ion formed near 0 eV possesses a lifetime exceeding 10 μs. According to *ab initio* calculations the geometrical structure of the ground state anion is considerably different from the neutral structure.